

**AFRL-PR-WP-TR-2002-2030**

**DEVELOPMENT OF THE PRESSURE-SENSITIVE PAINT (PSP) TECHNIQUE FOR ADVANCED TURBOMACHINERY APPLICATIONS**

**Kelly R. Navarra**

**Engine Integration and Assessment Branch (AFRL/PRTA)**

**Turbine Engine Division**

**Propulsion Directorate**

**Wright-Patterson Air Force Base, OH 45433-7251**



**May 1997**

**FINAL REPORT FOR PERIOD 01 JULY 1995 – 17 MAY 1997**

**Approved for public release; distribution unlimited.**

**20020517 077**


**PROPULSION DIRECTORATE  
AIR FORCE RESEARCH LABORATORY  
AIR FORCE MATERIEL COMMAND  
WRIGHT-PATTERSON AIR FORCE BASE, OH 45433-7251**


## NOTICE

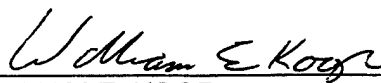
USING GOVERNMENT DRAWINGS, SPECIFICATIONS, OR OTHER DATA INCLUDED IN THIS DOCUMENT FOR ANY PURPOSE OTHER THAN GOVERNMENT PROCUREMENT DOES NOT IN ANY WAY OBLIGATE THE U.S. GOVERNMENT. THE FACT THAT THE GOVERNMENT FORMULATED OR SUPPLIED THE DRAWINGS, SPECIFICATIONS, OR OTHER DATA DOES NOT LICENSE THE HOLDER OR ANY OTHER PERSON OR CORPORATION; OR CONVEY ANY RIGHTS OR PERMISSION TO MANUFACTURE, USE, OR SELL ANY PATENTED INVENTION THAT MAY RELATE TO THEM.

THIS REPORT IS RELEASABLE TO THE NATIONAL TECHNICAL INFORMATION SERVICE (NTIS). AT NTIS, IT WILL BE AVAILABLE TO THE GENERAL PUBLIC, INCLUDING FOREIGN NATIONS.

THIS TECHNICAL REPORT HAS BEEN REVIEWED AND IS APPROVED FOR PUBLICATION.

  
\_\_\_\_\_  
KELLY R. NAVARRA  
PROJECT ENGINEER  
ENGINE INTEGRATION AND ASSESSMENT BRANCH  
TURBINE ENGINE DIVISION

  
\_\_\_\_\_  
JEFFREY M. STRICKER  
CHIEF  
ENGINE INTEGRATION AND ASSESSMENT BRANCH  
TURBINE ENGINE DIVISION

  
\_\_\_\_\_  
WILLIAM E. KOOP  
CHIEF OF TECHNOLOGY  
TURBINE ENGINE DIVISION  
PROPULSION DIRECTORATE

Do not return copies of this report unless contractual obligations or notice on a specific document require its return.

**REPORT DOCUMENTATION PAGE**Form Approved  
OMB No. 074-0188

Public reporting burden for this collection of information is estimated to average 1 hour per response, including the time for reviewing instructions, searching existing data sources, gathering and maintaining the data needed, and completing and reviewing this collection of information. Send comments regarding this burden estimate or any other aspect of this collection of information, including suggestions for reducing this burden to Washington Headquarters Services, Directorate for Information Operations and Reports, 1215 Jefferson Davis Highway, Suite 1204, Arlington, VA 22202-4302, and to the Office of Management and Budget, Paperwork Reduction Project (0704-0188), Washington, DC 20503

**1. AGENCY USE ONLY (Leave blank)****2. REPORT DATE**  
May 1997**3. REPORT TYPE AND DATES COVERED**  
Final, 07/01/1995 – 05/17/1997**4. TITLE AND SUBTITLE**

Development of the Pressure-Sensitive Paint (PSP) Technique for Advanced Turbomachinery Applications

**5. FUNDING NUMBERS**C: In-house  
PE: 62203F  
PR: 3066  
TA: OP  
WU: MT**6. AUTHOR(S)**

Kelly R. Navarra

**7. PERFORMING ORGANIZATION NAME(S) AND ADDRESS(ES)**Engine Integration and Assessment Branch (AFRL/PRTA)  
Turbine Engine Division  
Propulsion Directorate  
Wright-Patterson Air Force Base, OH 45433-7251**8. PERFORMING ORGANIZATION REPORT NUMBER**

AFRL-PR-WP-TR-2002-2030

**9. SPONSORING / MONITORING AGENCY NAME(S) AND ADDRESS(ES)**PROPULSION DIRECTORATE  
AIR FORCE RESEARCH LABORATORY  
AIR FORCE MATERIEL COMMAND  
WRIGHT-PATTERSON AIR FORCE BASE, OH 45433-7251  
POC: Kelly R. Navarra, AFRL/PRTA, (937) 255-5318**10. SPONSORING / MONITORING AGENCY REPORT NUMBER**

AFRL-PR-WP-TR-2002-2030

**11. SUPPLEMENTARY NOTES****12a. DISTRIBUTION / AVAILABILITY STATEMENT**

Approved for public release; distribution unlimited.

**12b. DISTRIBUTION CODE****13. ABSTRACT (Maximum 200 Words)**

A new pressure measurement technique that employs the tools of molecular spectroscopy has recently received considerable attention in the community. Measurements are made via oxygen-sensitive molecules attached to the surface of interest as a coating, or paint. The pressure-sensitive paint (PSP) technique is now commonly used in stationary wind tunnel tests; this thesis presents extension of the technique to advanced turbomachinery applications. New pressure- and temperature-sensitive paints (TSPs) have been developed for application to a state-of-the-art compressor where pressures up to 2 atm and surface temperatures to 140 °C are expected for the first stage rotor. PSP and TSP data images have been acquired from the suction surface of the first-stage rotor at 85 percent of the correct design speed for the compressor peak efficiency condition. The shock structure is clearly visible in the pressure image, and visual comparison to the corresponding computer prediction shows quantitative pressures similar to the PSP data. The measurement error is estimated to range from 0.36 kPa in low pressure regions to 4 kPa in high pressure regions.

**14. SUBJECT TERMS**

Pressure-sensitive paint

**15. NUMBER OF PAGES**

94

**16. PRICE CODE****17. SECURITY CLASSIFICATION OF REPORT**

Unclassified

**18. SECURITY CLASSIFICATION OF THIS PAGE**

Unclassified

**19. SECURITY CLASSIFICATION OF ABSTRACT**

Unclassified

**20. LIMITATION OF ABSTRACT**

SAR

NSN 7540-01-280-5500

Standard Form 298 (Rev. 2-89)  
Prescribed by ANSI Std. Z39-18  
298-102

## TABLE OF CONTENTS

LIST OF FIGURES	v
LIST OF TABLES	vi
ACKNOWLEDGEMENTS	vii
1.0 INTRODUCTION	1
2.0 BACKGROUND	3
3.0 MEASUREMENT CONCEPT	4
3.1 Luminescence	5
3.2 Fluorescence vs. Phosphorescence	8
4.0 MEASUREMENT TECHNIQUES	11
4.1 Luminescence Intensity	11
4.2 Luminescence Lifetime	14
5.0 PAINT DEVELOPMENT FOR TURBOMACHINERY APPLICATIONS	15
5.1 Luminescence Decay Time	16
5.2 Pressure and Temperature Requirements	18
5.3 Pressure and Spatial Resolution	20
6.0 PAINT-EVALUATION PROCEDURE	21
6.1 Stern-Volmer Relation	23
6.2 Pressure Resolution	26
7.0 PAINT PERFORMANCE	27
7.1 Stern-Volmer Calibration Results	27
7.2 Pressure Resolution	29

7.3	Effect of Oil on Paint Performance	33
8.0	APPLICATION TO A TRANSONIC ROTOR	35
8.1	Test-Article Description/Preparation	35
8.2	Test Setup	41
8.3	Data-Acquisition Procedure	45
8.4	Post-Processing Procedure	47
9.0	TRANSONIC-ROTOR RESULTS	51
10.0	CONCLUSIONS	57
	REFERENCES	60
	APPENDIX A: Previous PSP Experiences in Turbomachinery	67
	APPENDIX B: Timing Calculation for Derotation	73
	APPENDIX C: Paint-Calibration Data	74
	APPENDIX D: Compressor Research Facility Background	81

## LIST OF FIGURES

Figure 3.1	Jablonski Diagram	6
Figure 4.1	Time-Resolved Fluorescence of Pyrene	12
Figure 5.1	CFD Prediction, 85% Nc, Peak Efficiency	19
Figure 6.1	Paint Calibration Chamber	24
Figure 7.1	Performance of PSP Developed for Turbomachinery	28
Figure 7.2	Performance of TSP Developed for Turbomachinery	30
Figure 7.3	PSP Sensitivity to Pressure	31
Figure 7.4	PSP Percent Error in Pressure Measurement	32
Figure 7.5	Effect of Oil on Paint Performance	34
Figure 8.1	Compressor Schematic	36
Figure 8.2	Photograph of a Painted Compressor Blade	39
Figure 8.3	PSP Compressor Test Setup	42
Figure 8.4	Photograph of the Test Setup	44
Figure 8.5	Honeycomb Noise Pattern from ICCD Minifier	49
Figure 9.1	First-Stage-Rotor Image Region	52
Figure 9.2	Rotor 1 Suction-Surface PSP Wind-On Image	53
Figure 9.3	Flat-Field Corrected TSP Wind-On Image	54
Figure 9.4	Qualitative Rotor 1 TSP Image, 85% Nc, Peak Efficiency	55
Figure 9.5	Qualitative Rotor 1 PSP Image, 85% Nc, Peak Efficiency	56

Figure A.1	J79 Wind-On PSP Image	68
Figure A.2	J79 Chordwise Plot of PSP Data	69
Figure A.3	Painted Transonic Rotor	71
Figure A.4	Transonic-Rotor PSP Image	72
Figure C.1	Performance of Original PSP Formula	75
Figure D.1	Compressor Research Facility Layout	82
Figure D.2	Test Chamber Layout	83

## LIST OF TABLES

Table 5.1	High-Speed Rotor Design Conditions	17
Table 5.2	Paint Requirements for Turbomachinery	22
Table 8.1	Airfoil Geometry Parameters for Rotor 1	38

## ACKNOWLEDGEMENTS

The author recognizes Mr. David Car and Drs. Douglas Rabe and Steven Puterbaugh for support of this effort and the employees of the Turbine Engine Research Center (TERC), Wright Laboratory, for their support, guidance and assistance with post-processing during the compressor test. Dr. James Gord of the Fuels and Lubrication Division of Wright Laboratory is acknowledged for his invaluable contributions in establishing this research effort. Special thanks go to Dr. Larry Goss of Innovative Scientific Solutions, Inc. (ISSI), who accepted the difficult task of developing a paint suitable for the harsh turbomachinery environment. Messrs. Keith Grinstead and Darryl Trump of ISSI are acknowledged for their exhaustive efforts involving the experimental setup and data acquisition during the paint development and the compressor test. Mr. Marvin Sellers of Sverdrup Technologies, Arnold Engineering and Development Center (AEDC), provided the author the opportunity to conduct the ground work required to establish the Wright Laboratory pressure-sensitive-paint program. Special thanks go to Drs. Walter O'Brien and Clinton Dancey of Virginia Tech for their valuable instruction which afforded the author an appreciation of the world of turbomachinery and for their technical feedback throughout the course of this research.



## 1.0 INTRODUCTION

Turbomachinery components in jet engines are becoming extremely complex and highly three dimensional in an effort to achieve increased performance over a wide range of operating conditions. Evaluation of these advanced designs requires improved understanding of the flow behavior, and advanced diagnostic techniques are needed to acquire the desired benchmark experimental data. These new measurement capabilities must be pursued in conjunction with design-system improvements to meet future propulsion-system requirements.

The aerodynamic and aeroelastic performance of turbomachinery blades and vanes is dependent on steady-state and transient surface-pressure distributions. Adverse pressure gradients and large-amplitude fluctuations can lead to unacceptable aerodynamic and aeroelastic instabilities. Currently, blade-mounted pressure transducers are used to measure surface pressure. However, such transducers cover a limited region ( $< 5\%$ ) of the blade surface and result in some compromise to the structural integrity of the blade. Typically these transducers have limited reliability in full-scale turbomachinery environments. For these reasons, improved blade-surface pressure-measurement techniques are needed to aid the understanding of flow behavior in turbomachinery components.

A relatively new technique that employs the tools of molecular spectroscopy to measure pressures optically is the subject of this thesis. Measurements are made via photoluminescent oxygen-sensitive molecules attached to the surface of interest as a

coating, or paint; hence, the technology is referred to as pressure-sensitive paint (PSP). Although a number of PSPs are currently available they were engineered for use in stationary wind-tunnel tests and do not meet the pressure and temperature requirements of turbomachinery applications. The objective of this research effort was to develop a PSP suitable for the turbomachinery environment and to demonstrate the measurement technique for turbomachinery applications. Technical challenges, aside from development of the paint, involve the crucial alignment of data images and the temperature correction of the PSP data. Proper alignment of the reference- and test-condition images and the application of a field-temperature correction are the keys to extracting quantitative data from the PSP.

This thesis begins with a brief discussion of the theory of luminescence and dynamic quenching, followed by a presentation of the general methods of acquiring data from the oxygen-sensitive molecules (lumiphores). Subsequent sections discuss the establishment of paint-performance requirements for turbomachinery applications, procedures for evaluating various paints, and performance results of the paints developed during this research effort. The remaining sections will describe application of the developed technology to a state-of-the-art transonic compressor as well as the techniques used to align the reference and wind-on images and to correct for temperature effects. Quantitative results acquired from the suction surface of the first-stage rotor operating at 85%  $N_c$ , at the peak-efficiency condition will be presented for both the temperature-sensitive paint (TSP) and the PSP. These results will be discussed and future work planned for this research area will be identified.

## 2.0 BACKGROUND

Photoluminescence was first used as a tool for flow visualization in 1980 by Peterson and Fitzgerald (1). Unfortunately, the significance of the experiment was dismissed because the oxygen sensitivity of the fluorescent dye and the oxygen permeability of the binding medium were poor. Over the following decade, paint performance improved, charge-couple-device (CCD) cameras evolved, and digital hardware advanced to a level where the use of photoluminescence to obtain optical surface-pressure measurements became practical.

Early developments of the pressure-sensitive paint (PSP) technique were initiated at the Central Aero-Hydrodynamics Institute in Moscow (TsAGI) and the University of Moscow in the mid-1980's (2,3,4). TsAGI developed a commercial PSP system jointly with the Italian firm INTECO (5,6). European researchers such as the Deutsche Forschungsanstalt für Luft- und Raumfahrt e.V. (DLR) began PSP efforts using the INTECO system but have since initiated an independent PSP program (7,8). Also, TsAGI recently formed OPTROD, Ltd., to market their paint formulations (9,10) in an operation separate from INTECO. Other independent PSP efforts in Europe now include Rolls Royce (11) and the Office National d'Etudes et de Recherches Aéronautiques (ONERA) (12).

In the United States, McLaughlan and Bell at NASA Ames Research Center, in collaboration with the University of Washington, have made contributions to development of the technique since the late 1980's (13-18). Efforts were also initiated at McDonnell

Douglas Aerospace in 1990 (19,20,21), and Purdue University (22,23,24) and NASA Langley (25,26,27) began PSP development efforts in the early 1990's. In the mid-1990's the University of Florida branched out of the McDonnell Douglas program (28,29). Around this time, Arnold Engineering and Development Center (AEDC) (30), Wright Laboratory (WL) (31), and NASA Lewis (32) initiated paint programs. Of all the PSP efforts mentioned, WL and Purdue are the only programs which address PSP development for advanced turbomachinery applications. Undoubtedly many of organizations are not mentioned here which have either used the PSP technique through collaboration with one of the above organizations or initiated independent programs. Certainly the number of institutions which are interested in PSP is increasing because of the attractiveness of the high-resolution, low-cost measurement.

### **3.0 MEASUREMENT CONCEPTS**

Knowledge of the reversible relationship that exists between the luminescence of particular molecules and the oxygen concentration dates back to the late 1930's (33). Since the measured oxygen concentration is directly related to the partial pressure of air at a given temperature, pressure can be accurately determined based upon the luminescence behavior of these molecules. Although this tool has been used primarily in the biomedical field, engineers now apply the technology to aerodynamic surfaces to acquire global pressure measurements under test conditions. To date, numerous studies have been conducted in efforts to better understand and utilize luminescence quenching. A

discussion of the relationship among these luminescent molecules, oxygen concentration, and local pressure is in order.

### 3.1 Luminescence

Two luminescence processes, phosphorescence and fluorescence, can be effectively utilized to quantitate oxygen. Each of these is described in the context of the Jablonski energy-level diagram for a typical lumiphore, as depicted in Fig. 3.1 (34). This diagram is arranged to display electronic and vibrational energy levels, with lower energy states appearing at the bottom of the figure and higher energy states appearing at the top. Relevant photophysical processes associated with a typical pressure-measurement sequence can be described through the use of this diagram.

Absorption (a) occurs when the lumiphore is exposed to electromagnetic radiation of appropriate energy (i.e., frequency). During this process electrons are promoted from the ground vibrational state of the  $S_0$  electronic manifold to excited vibrational states in the  $S_1$  and  $S_2$  electronic manifolds. Higher lying excited electronic states not depicted in Fig. 3.1 may be populated as well. Once it exists in an excited state, the lumiphore may undergo a number of processes to return to its stable, lowest energy configuration. These deactivation processes can be broadly grouped into two general categories: 1) non-radiative deactivation processes in which the excess energy associated with the absorbed photon is transferred to the surrounding medium, and 2) radiative deactivation processes in which the excess energy is emitted as light.

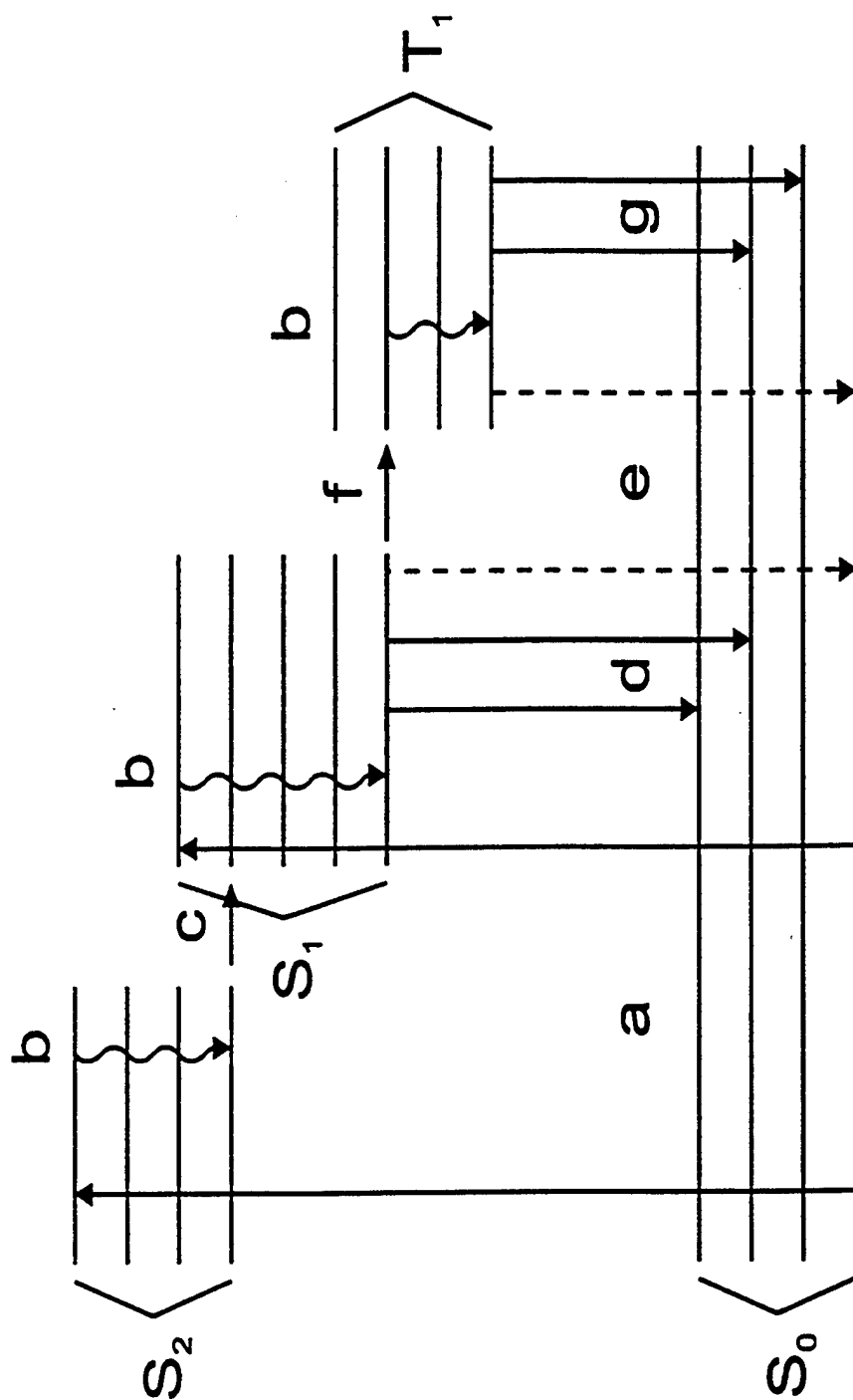


**FIGURE 3.1** Jablonski diagram depicting the vibrational and electronic states and the photophysical processes associated with a typical lumiphore.

Immediately following the absorption or excitation event (a), the excited lumiphore relaxes to the lowest energy vibrational state of the excited electronic state ( $S_1$  and/or  $S_2$ ) through vibrational relaxation (b) in which excess vibrational energy associated with the lumiphore is transferred to the thermal motion of the surrounding medium. Vibrational relaxation in the  $S_2$  manifold (or in higher lying excited electronic manifolds) is followed by internal conversion (c) to lower lying excited electronic states. This non-radiative process couples states of the same multiplicity (multiplicity describes the number of unpaired electrons associated with a particular energy state). In this example  $S_1$  and  $S_2$  are singlet states, i.e., states in which the valence electrons are fully paired. Through non-radiative sequences of internal conversion and vibrational relaxation, the excited lumiphore rapidly relaxes to the lowest vibrational state of the  $S_1$ -excited electronic state.

From this energy state the molecule may undergo a number of different processes. Under some circumstances internal conversion to the ground electronic state,  $S_0$ , with subsequent vibrational relaxation is an important deactivation mechanism. However, fluorescence (d) and external conversion (e) through dynamic quenching are the key processes associated with measurements based on PSPs. Fluorescence is a luminescence process that couples states of the same multiplicity. During this process excess energy is emitted as photons to yield lumiphores in the ground electronic manifold. External conversion is a non-radiative process that competes with fluorescence for deactivation of the  $S_1$  excited electronic state. External conversion through dynamic quenching occurs when oxygen molecules collide with the excited lumiphore, and energy is transferred

from the lumiphore to the oxygen-quenching molecules. The competition between fluorescence and external conversion (dynamic quenching) permits the quantification of oxygen.

In addition to internal conversion, external conversion, and fluorescence, the  $S_1$ -excited lumiphore can undergo intersystem crossing (f)—a process in which the excited singlet state couples to a triplet state,  $T_1$ . This event involves a change in multiplicity from the singlet state in which the valence electrons are fully paired to a triplet state in which two electrons are unpaired. The vibrationally relaxed  $T_1$  state can couple to  $S_0$  through intersystem crossing, external conversion (dynamic quenching), or phosphorescence (g). The first two processes are non-radiative, while the last involves photon emission. Once again, the competition between dynamic oxygen quenching and phosphorescence can be used to quantitate oxygen concentration.

It is important to note that the Jablonski diagram and the photophysical processes identified in this discussion best describe the characteristics of “well-behaved” organic lumiphores in liquid solution. While it provides an excellent description of the spectroscopic behavior of luminescent molecules, this model should be applied with caution to the prediction of the behavior of specific PSP formulations. Organometallic lumiphores immobilized in solid matrices can display somewhat different characteristics.

### 3.2 Fluorescence vs. Phosphorescence

Clearly, several important differences exist in the underlying photophysics associated with fluorescence and phosphorescence. Specific differences in these processes



involve timescales, sensitivities to dynamic quenching, sensitivities to temperature, and spectral-emission characteristics. Each of these luminescence processes has advantages and disadvantages when utilized for optical pressure measurements.

The events that result in fluorescence emission involve fully allowed spectroscopic transitions that occur between states of the same multiplicity. As a result, the timescale for spontaneous fluorescence typically ranges from  $10^{-10}$  to  $10^{-6}$  s. Phosphorescence, on the other hand, involves transitions that require a change in multiplicity and are, therefore, quantum-mechanically forbidden. Phosphorescence occurs on a timescale ranging from  $10^{-4}$  to  $10^4$  s as a consequence of this spectroscopic restriction. This enormous difference in emission timescales has significant implications for the application of optical pressure-measurement techniques to the study of transient or unsteady phenomena. It is also important to note the effects of differences in dynamic quenching on these processes. Quenching deactivates  $S_1$  to compete with fluorescence and deactivates  $T_1$  to compete with phosphorescence. Because of the long timescales associated with phosphorescence, dynamic quenching that occurs at a given bimolecular quenching rate has a more pronounced effect on a phosphorescence signal than on a fluorescence signal. The long lifetime of the  $T_1$ -excited electronic state increases the likelihood that quenching collisions will take place. In other words, quenching competes more effectively with the slower phosphorescence process than with the faster fluorescence process. This lifetime dependence is treated formally in the Stern-Volmer kinetic model described below.

These differences in sensitivity to dynamic quenching have two important implications. First, phosphorescence measurements of oxygen--and, therefore, pressure--are more sensitive than fluorescence measurements. For a given change in oxygen concentration, the change in phosphorescence intensity is greater than that in fluorescence intensity. As a result, phosphorescence measurements permit the experimental resolution of smaller changes in absolute pressure. The second implication involves the effects of temperature on the two processes. Dynamic quenching rates increase with temperature. As a result phosphorescence, which is more sensitive to dynamic quenching, is also more sensitive to fluctuations in temperature. In a paint formulation designed for the measurement of temperature fields, this is a desirable quality; however, this increased sensitivity to temperature can be problematic when making pressure measurements with a phosphorescence-based paint, as noted above.

Differences in timescale and dynamic-quenching sensitivity must be considered when designing a pressure-sensitive measurement scheme. In fact, the selection of a luminescence process for a particular pressure measurement will likely involve a tradeoff between optimizing pressure sensitivity (phosphorescence) and time response (fluorescence). In the case of turbomachinery applications, the timescales associated with phosphorescence are incompatible with the timing schemes required to stop the rotating image; as will be discussed in a later section

## 4.0 MEASUREMENT TECHNIQUES

The effects of dynamic oxygen quenching on luminescence emission are evident in both the intensity and the duration of the observed fluorescence or phosphorescence signal. Figure 4.1 demonstrates the time-resolved effects of pressures (10 - 175 kPa) on the fluorescence from a PSP employing pyrene. A dramatic change in fluorescence lifetime and integrated intensities with increasing pressure is observed in the raw signals. In practice, either the intensity or the lifetime of luminescence emission can be employed to quantitate oxygen concentration.

### 4.1 Luminescence Intensity

Traditionally, an intensity-based measurement method has been used to acquire PSP data because two-dimensional information can be obtained with a simple setup. In an intensity-based Stern-Volmer model, the effects of dynamic oxygen quenching on the luminescence intensity of a photoexcited probe molecule are described by:

$$\frac{I_0}{I} = 1 + K_q P_{O_2} \quad (1)$$

where  $I$  is the measured luminescence intensity,  $I_0$  is the luminescence intensity in the absence of oxygen quenching,  $P_{O_2}$  is the partial pressure of oxygen, and  $K_q$  is the Stern-Volmer constant. The first step in applying this model to practical measurements involves recording the luminescence lifetime as a function of oxygen concentration under controlled conditions to calibrate the model and extract a value for  $K_q$ , which represents the sensitivity of the measurement.

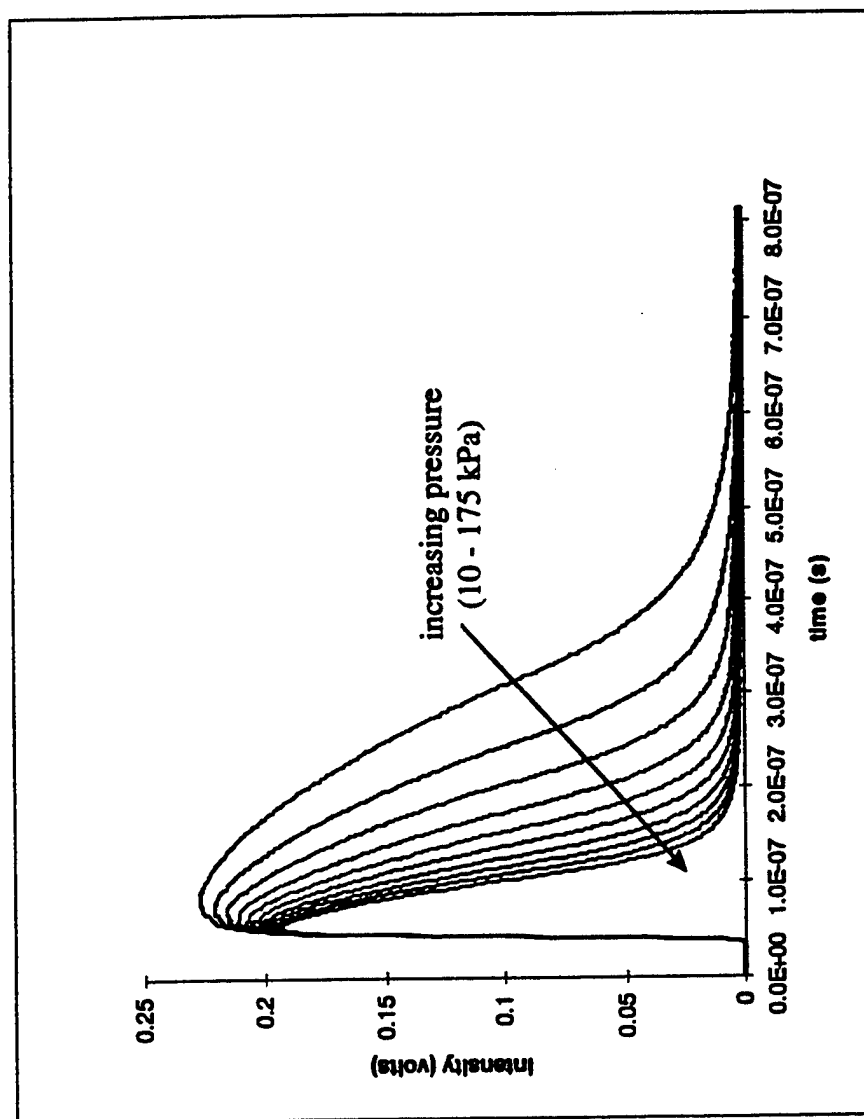


**Figure 4.1** Time-resolved fluorescence signals from a PSP employing pyrene.

Analysis of the Stern-Volmer kinetic model reveals that the Stern-Volmer constant,  $K_q$ , is given by the product of the unquenched luminescence lifetime,  $\tau_0$ , of the selected lumiphore and the bimolecular collisional quenching rate,  $k_q$ :

$$K_q = \tau_0 k_q. \quad (2)$$

This observation quantitatively describes the dependence of the dynamic quenching sensitivity on the luminescence lifetime and explains the difference in the sensitivity of fluorescence and phosphorescence. Because fluorescence lifetimes are shorter,  $K_q$  is smaller and fluorescence is less sensitive to dynamic quenching.

In the application of a Stern-Volmer model to the performance of pressure-field measurements, the luminescence intensity at a reference condition,  $I_{REF}$ , must be determined. This reference intensity is typically acquired over the surface of interest under quiescent conditions at 1 atm,  $P_{REF}$ , and is commonly referred to as the "wind-off" condition. When the luminescence intensity at a given test condition,  $I$ , is measured over the area of interest ("wind-on" image), the ratio of the measured intensities yields the desired pressure information:

$$\frac{I_{REF}}{I} = 1 + K_q \frac{P}{P_{REF}}. \quad (3)$$

The ratio of the luminescence intensities  $I$  and  $I_{REF}$  not only provides the desired pressure data but also effectively eliminates signal dependence associated with non-uniformities in lumiphore concentration and illumination. Intensities are generally sampled over the area of interest using some type of detector array such as a charge-coupled-device (CCD)

camera. The output of the array can be visually represented as an image, with the luminescence intensity displayed in pseudo-color or gray scale.

When this technique is used to measure the pressure on aerodynamic surfaces, model displacement often occurs between acquisition of the reference- (“wind-off”) and test- (“wind-on”) condition images. Thus, one of the most important requirements associated with intensity-based pressure measurements is careful alignment of these two images before the luminescence-intensity values are ratioed. Correct alignment can be achieved through the use of small circular marks placed directly on the model; these marks are visible in both the reference and test images. After alignment is complete, the image-intensity ratio is determined, equation 3 is applied, and the pressure is evaluated over the entire image plane on a pixel-by-pixel basis.

## **4.2 Luminescence Lifetime**

As mentioned previously, oxygen concentration can also be quantified based upon the lifetime of the lumiphore. In this case the luminescence lifetime can be determined by using a pulsed light source and recording the observed luminescence as a function of time (time-resolved measurement). Alternatively, an amplitude-modulated light source can be employed and the lifetime extracted from frequency-domain measurements of the luminescence intensity (phase-resolved measurement). In either case, the relevant Stern-Volmer kinetic model based upon lifetime measurements is represented by equations 4 and 5:

$$\frac{\tau_o}{\tau} = 1 + K_q P_{O_2} \quad (4)$$

$$\frac{\tau_{REF}}{\tau} = 1 + K_q \frac{P}{P_{REF}} \quad (5)$$

where  $\tau$ ,  $\tau_o$ , and  $\tau_{REF}$  are luminescence lifetimes under the test condition, in the absence of quenching, and at  $P_{REF}$ , respectively ( $K_q$  was discussed previously). The advantage of the lifetime technique over intensity-based measurements is that since the measured decay time is independent of variations in paint thickness and illumination, a wind-off reference condition is not required which simplifies post-processing. A potential disadvantage is the complexity associated with acquiring time- or frequency-domain data. Lifetime-based measurements are typically limited to a time-correlated single-point measurement (22,23,24); however, a new lifetime-based technique which utilizes two imaging detectors to achieve two-dimensional measurements is currently under development at Wright Laboratory. Since this new technique is not yet well established, the traditional intensity method for acquiring two-dimensional measurements was used in the present study.

## 5.0 PAINT DEVELOPMENT FOR TURBOMACHINERY APPLICATIONS

Based upon previous experience using PSP in rotors (discussed in Appendix A), it was recognized that the goal of extending the usefulness of this new measurement technique to steady-state applications in turbomachinery could not be achieved until paint performance was improved. Needed improvements included the extension of the

operational pressure and temperature range—with adequate pressure resolution to resolve flow phenomena. The paint was also required to have minimal temperature sensitivity, to adhere to the blade, and to provide an adequate signal-to-noise ratio (SNR). The response time of the paint also became an issue for transient applications. Table 5.1 shows the design condition of a full-scale transonic compressor (35). In the following paragraphs, the paint-performance requirements for acquiring quantitative data from the first stage of this state-of-the-art transonic compressor are identified.

### 5.1 Luminescent Decay Time

The first requirement involves the fluorescent decay time (or lifetime) of the paint. This issue surfaces when the application requires critical timing, as with turbomachinery or when the flow phenomenon is transient, or both. In the case where a rotating image must be stopped, it is important to know the time required between excitation and the requisite data acquisition as well as the luminescent decay time of the paint. It is desirable that the lifetime of the signal be approximately equal to the data-acquisition window (gate time) for maximizing the signal. On the other hand, the gate time must be sufficiently small to stop the rotating image. The gate time required to stop the blade motion for a 1-mm spatial resolution is  $\sim 2 \mu\text{s}$ , as calculated in Appendix B. Therefore, the paint in this particular application must contain fluorescent compounds ( $10^{-10}$  -  $10^{-6}$ ) because phosphorescent lifetimes ( $10^{-4}$  -  $10^4$ ) are too long to be compatible with the timing requirements for the intended rotor application.



**Table 5.1** First-stage-rotor design conditions from reference 35.

Parameter	Value
Design Speed	13,288 rpm
Total Pressure Ratio	2.5
Total Temperature Ratio	1.3
Mass Flow	71.8 kg/sec
Rotor Radius	35.24 cm

## 5.2 Pressure and Temperature Requirements

Figure 5.1 shows the computational-fluid-dynamics (CFD) prediction of the pressure on the suction surface of the first-stage rotor at 85% corrected speed under the peak-efficiency test condition. The CFD code was developed by NASA Lewis (36). Similarly, the code predicted the surface-static-temperature distribution across the blade (not shown). These data were extrapolated to define the required paint-performance range of 0.3 - 2 atm and -10 to +140°C. Of these two requirements, the temperature is more difficult to achieve because the most common lumiphores cannot survive beyond 100°C. The temperature sensitivity of the dynamic quenching rate,  $k_q$ , of lumiphores in solution was discussed in Section 3.2; however, PSPs are also affected by the binder in which the lumiphore is suspended. The solubility of oxygen in the binder, according to Henry's Law, is an additional temperature effect which must be taken into account for PSPs. Theoretically these effects could be engineered to cancel each other, but that would be a difficult task. Although minimization of the temperature dependence of the PSP is a design goal, it is unlikely a paint which is completely insensitive to temperature can be developed. If the temperature gradient is small, as it is for many wind-tunnel applications, a gross temperature correction can be used to produce acceptable results. However, applications with large temperature gradients, such as turbomachinery, require a temperature-sensitive paint, or other temperature-sensing techniques, that will allow more detailed temperature corrections. Several organizations are investigating the development of a dual-lumiphore paint where two scalars, pressure and temperature, can

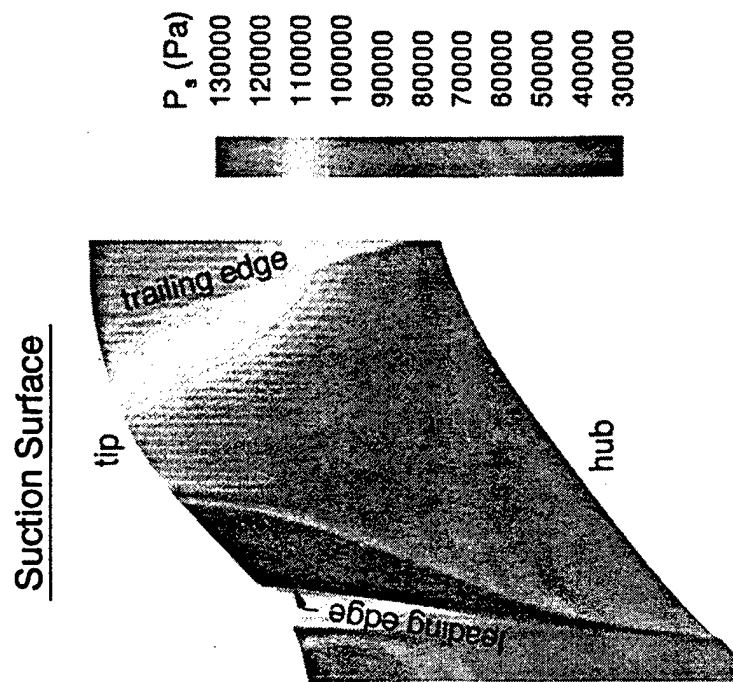


**Figure 5.1** CFD surface-pressure prediction at 85%  $N_c$ , peak-efficiency operating condition.

be measured. However, a dual-lumiphore paint is not necessary for the subject application where multiple blades can be painted.

### **5.3 Pressure and Spatial Resolution**

The ultimate goal of PSP development would be to provide a measurement having higher spatial and pressure resolution than currently available with blade-mounted pressure transducers. Despite its importance, spatial resolution is really not an issue in a comparison of PSPs and pressure transducers. When pressure transducers are used, very few are mounted on blades because of the high cost and risk of compromise to the structural integrity of the blade. In the case of PSP, the spatial resolution is limited only by the detection device. With current CCD cameras having a million or more pixels, PSP provides unequaled spatial resolution.

To define the performance requirements of PSP in the areas of spatial and pressure resolution, the state-of-the art of blade-mounted pressure transducers was assessed. Reference 37 describes the digitization procedure used for the blade-mounted pressure-transducer data reported in reference 38. Here, the data-reduction process provided a pressure measurement having a resolution of 17.1 Pa, with an uncertainty of 3.17 kPa (37). In the test described in reference 38, seven pressure transducers were mounted along the chordline at 85% span, which is approximately equivalent to one pressure measurement every 25.4 mm. Thus, to compete with pressure transducers, PSP must provide pressure and spatial resolutions of  $> 3.17$  kPa and one measurement per 25.4 mm, respectively. Measurement accuracy 0.34 kPa (0.05 psi) has been reported

using PSPs (39). However, these accuracies were obtained in well-controlled test environments, whereas in most applications model movement and temperature gradients significantly affect the measurement errors.

Table 5.2 summarizes the paint-performance requirements defined in this section. One obvious requirement not discussed is the ability of the paint to adhere to the blade. Unfortunately, the conditions of the actual compressor are difficult to reproduce in a simple laboratory experiment. Thus, the only means of evaluating the adhesive qualities of the paints prior to the compressor test is through visual comparison to other paints which survived previous rotor tests (reported in Appendix A).

## **6.0 PAINT-EVALUATION PROCEDURE**

Several PSPs are currently available. However, these paints were engineered for stationary wind-tunnel applications which are primarily steady state which involve small temperature gradients. Therefore, most of these paints utilize phosphorescence--despite the temperature sensitivity--to take advantage of the increased sensitivity to pressure resulting from the long luminescent decay of phosphorescence. As discussed earlier, turbomachinery requires the short decay time of fluorescent materials. Therefore, a fluorescent PSP is required for turbomachinery applications. A temperature-sensitive paint (TSP) is also needed to provide a means for temperature-correcting the PSP data. The following paragraphs describe the experiments and procedures used in the

**Table 5.2** Pressure-sensitive paint requirements for first-stage transonic rotor.

<b>Parameter</b>	<b>Value</b>
Pressure Range	0.3 to 2.0 atmospheres
Temperature Range	-10 to 140 °C
Decay Time	<2.1 $\mu$ s (Fluorescent molecule)
Spatial Resolution	>1 measurement per 2.54 cm
Pressure Resolution	<3.17 kPa

development and evaluation of the performance of new TSP and PSP formulations for turbomachinery.

### 6.1 Stern-Volmer Relation

The pressure and temperature characteristics of the paint are dictated by the Stern-Volmer relation described in equation 5. The Stern-Volmer constant,  $K_q$ , is experimentally determined with the use of a vacuum chamber. The chamber employed in this study was the cross pipe shown schematically in Fig. 6.1. Quartz windows are located in two adjacent flanges. The nitrogen laser beam (337 nm, 100  $\mu$ J, 200-ps pulse at 10 Hz) is split to trigger the digital oscilloscope by means of a photodiode. The remainder of the beam passes through a neutral density filter and is turned by a mirror to impinge on the paint sample through the first quartz window. The sample is mounted at 45°, and the resulting fluorescent signal exits through the second window. The signal is passed through an ultra-violet filter to remove reflected laser light. If the sample is the TSP, then a blue filter must be placed behind the ultra-violet filter to remove an emission band of photons which are not temperature sensitive. The photomultiplier tube detects the fluorescent signal after passing through collection optics and sends the trace (triggered by the photodiode) of the decay to the sampling oscilloscope.

The computer establishes the pressure and temperature environment of the calibration chamber by means of a digital pressure controller and thermal-electric temperature controller. The paint sample is mounted on the thermal-electric heater (TEH), and two set screws fitted with ceramic sleeves are used to secure the paint

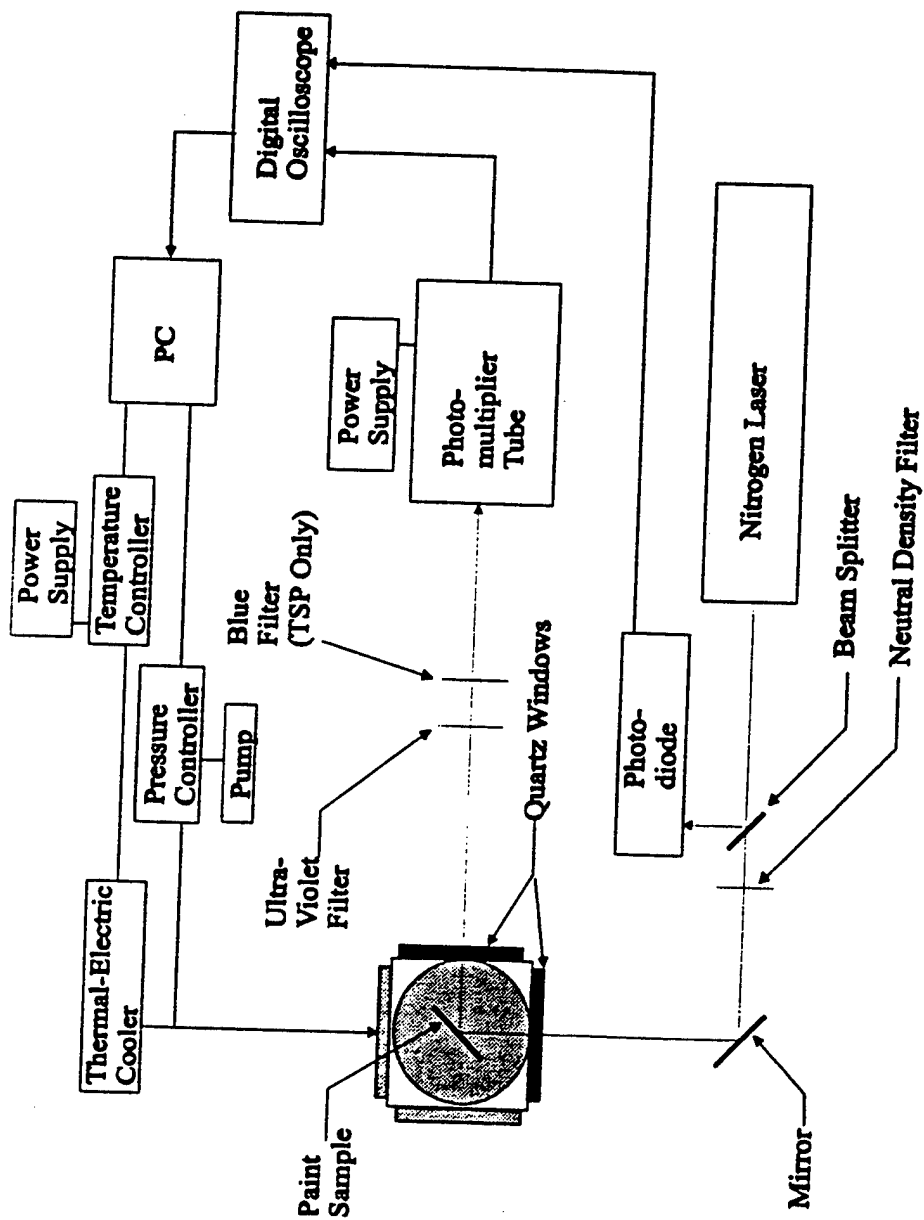


Figure 6.1 Paint calibration chamber.



sample. Thermal-electric grease is used to provide good contact between the paint sample and the TEH. A K-type thermocouple is placed in contact with the paint surface between the sample and one of the ceramic sleeves. Again, thermal-electric grease is used to provide sufficient contact. The pressure of the calibration unit could be varied from 10 to 199 kPa, and the surface temperature of the sample could be varied from -15 to 150°C.

For determining the Stern-Volmer relation, the calibration unit is run by a simple computer program (PSP) written using CVI; the user inputs the desired pressure and temperature range over which the sample will be tested and indicates the number of data points and the number of traces averaged for each point. Early in the paint-development cycle, the pressure was set to range from 10 to 175 kPa using 10 points, and the temperature was set to range from room temperature to 150°C using 13 points. The number of traces acquired for each average was consistently set to 128. This test matrix consisted of 130 points which required 5 hr for completion. Final calibrations would extend the temperature to -10° and the pressure to 200 kPa.

For each temperature an ASCII file was created which recorded the temperature, the pressure readings, and the corresponding integrated intensity of the decay curve. The integration assumed an exponential decay, with the limits being defined as 20 and 80% of the decay. These data were then imported into an Excel spreadsheet for plotting, and a polynomial-curve-fitting macro was applied to determine the Stern-Volmer equation.

The process of developing a new T/PSP merely involved the calibration of hundreds of binder and luminophore combinations over the desired pressure and temperature range.

## 6.2 Pressure Resolution

A first estimate of the pressure sensitivity and error of the PSP measurement can be obtained from the derivative of the Stern-Volmer equation. The derivation below follows that presented by Oglesby in reference 40. However, the Wright Laboratory paints display a second-order relationship between pressure and luminosity rather than the classical linear Stern-Volmer relation reported in equation 3 and by Oglesby. The Stern-Volmer equation for the Wright Laboratory paint has the form:

$$\left[ \frac{I_{REF}}{I} \right]_P = A + BP + CP^2 \quad (6)$$

where the coefficients A, B, and C are functions of temperature. For simplicity, the temperature will be considered a constant, known source. Applying the first- and second-order derivatives with respect to pressure to the inverted Stern-Volmer equation yields the paint sensitivity to pressure ( $S_P$ ):

$$I_{RP} = \left[ \frac{I}{I_{REF}} \right]_P \quad (7)$$

$$S_P = \frac{dI_{RP}}{dP} = -\frac{(B + 2CP)}{(A + BP + CP^2)^2} \quad (8)$$

where  $I_{RP}$  is the measured emittance and  $S_P$  is the sensitivity to pressure. This equation is solved for  $dP$  and normalized to pressure to yield the percent error in pressure ( $E_P$ ):

$$E_P = \frac{\Delta P}{P} = \frac{(A + BP + CP^2)^2}{(B + 2CP)P} * \Delta I_{RP} \quad (9)$$

where  $\Delta I_{RP}$  is the estimated error in measured emittance. The same procedure can be used to estimate the sensitivity to temperature and errors in temperature measurement of the TSP where the TSP relationship between intensity and temperature has the form:

$$\left[ \frac{I_{REF}}{I} \right]_T = d_1 + d_2 T + d_3 T^2 + d_4 T^3 + d_5 T^4 \quad (10)$$

## 7.0 PAINT PERFORMANCE

Through the use of the calibration chamber, Wright Laboratory was able to develop a new PSP that was better suited for turbomachinery applications. Numerous paint formulations composed of various binders and solvents were tested as well as methods of application and surface treatments. Common problems that resulted in the failure of a paint formulation were instability of the matrix, which was found to be the primary threat to photo-instability, and lack of pressure sensitivity.

### 7.1 Stern-Volmer Calibration Results

The first PSP developed for turbomachinery displayed a 29% decrease in temperature sensitivity compared to typical phosphorescence-based paints; however, this paint experiences a complete loss of pressure sensitivity after 80°C. These results are presented in Appendix C. Development continued in an attempt to increase the temperature capability of the paint. Figure 7.1 displays the performance of this paint. As

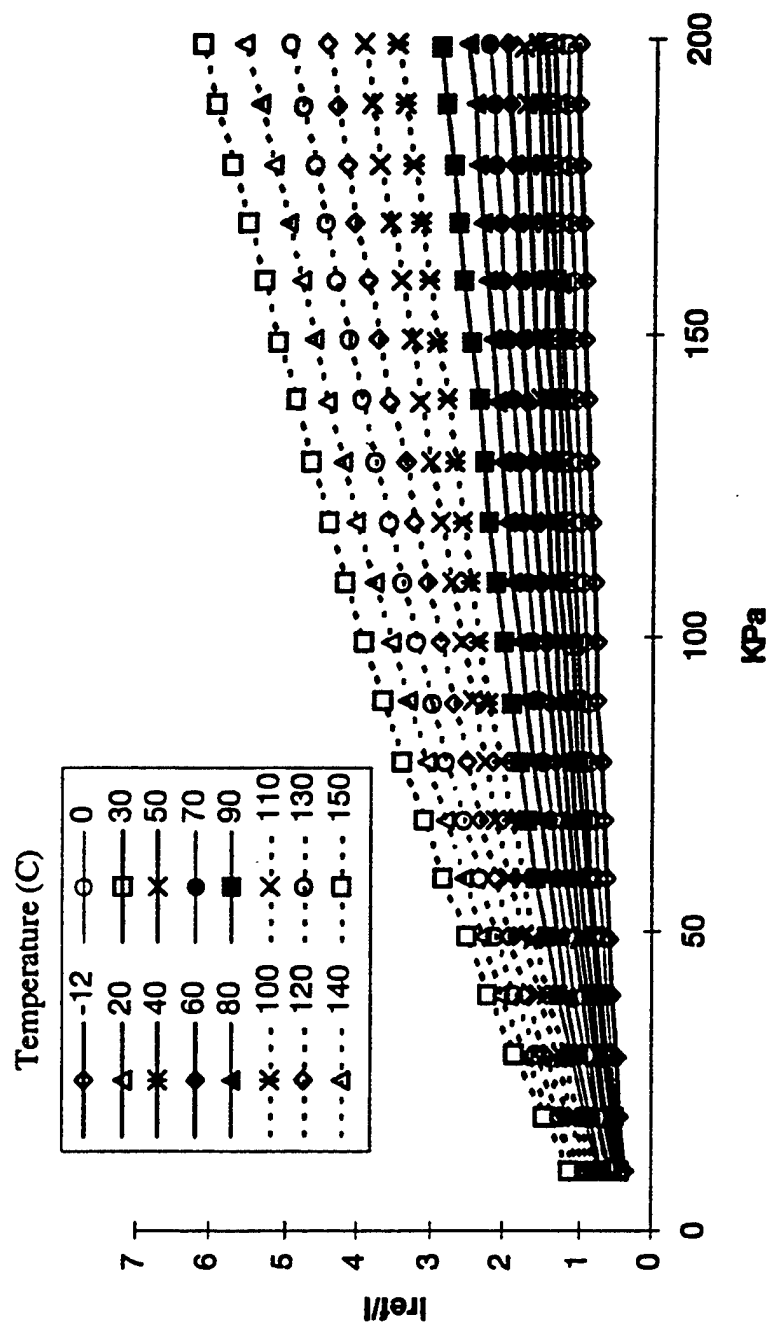


Figure 7.1 Performance of PSP developed for turbomachinery.

the figure shows, the PSP survives temperatures to 150°C and pressures to 200 kPa (~2 atm). This formula displayed a 42% decrease in temperature sensitivity compared to typical phosphorescence-based paints.

The effect of temperature on the dynamic quenching is apparent in the data presented. A sixth-order polynomial curve fit was required for sufficient modeling of the temperature dependence of the calibration coefficients A, B, and C presented in equation 6. Pressure sensitivity generally increases with temperature--an increase of 22% is observed from 60°C to 150°C in Fig. 7.1. The TSP developed proved suitable for the rotor test, as shown in Fig. 7.2. The TSP was insensitive to pressure, and the fourth-order polynomial curve fit to temperature (presented in equation 10) sufficiently modeled the data.

## **7.2 Pressure Resolution**

Figures 7.3 and 7.4 display the results for the sensitivity and error equations presented in Section 6.2 for an estimated measured-emittance uncertainty of 1%. The PSP data are shown for various temperatures to demonstrate the effect of temperature on error. On the average, an increase in temperature of 5°C caused an increase in the pressure error of 0.13% at 1 atm. The pressure error for the PSP also increased with pressure. The TSP data (not shown) displayed an 0.08% increase in the temperature error for every 5°C increase in temperature. Unfortunately, in a compressor the areas of highest pressure are also those of highest temperature. Temperature/pressure

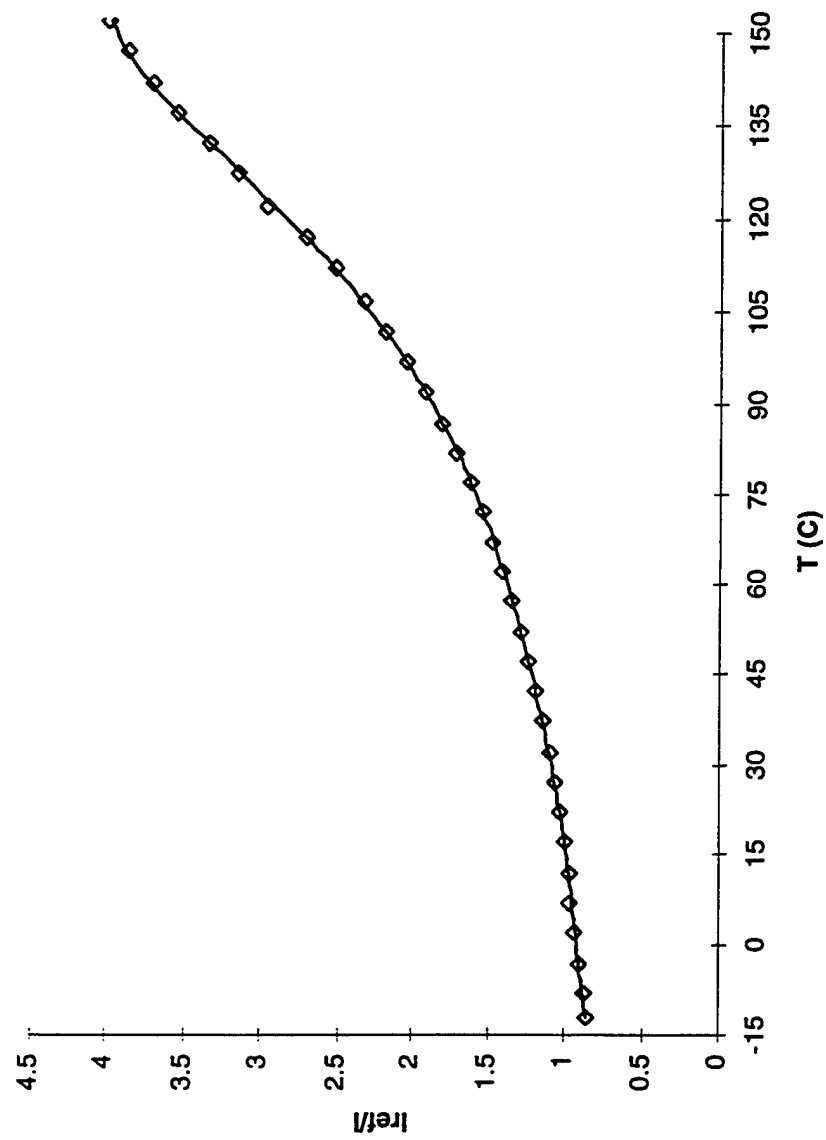


**Figure 7.2** Performance of TSP developed for turbomachinery.

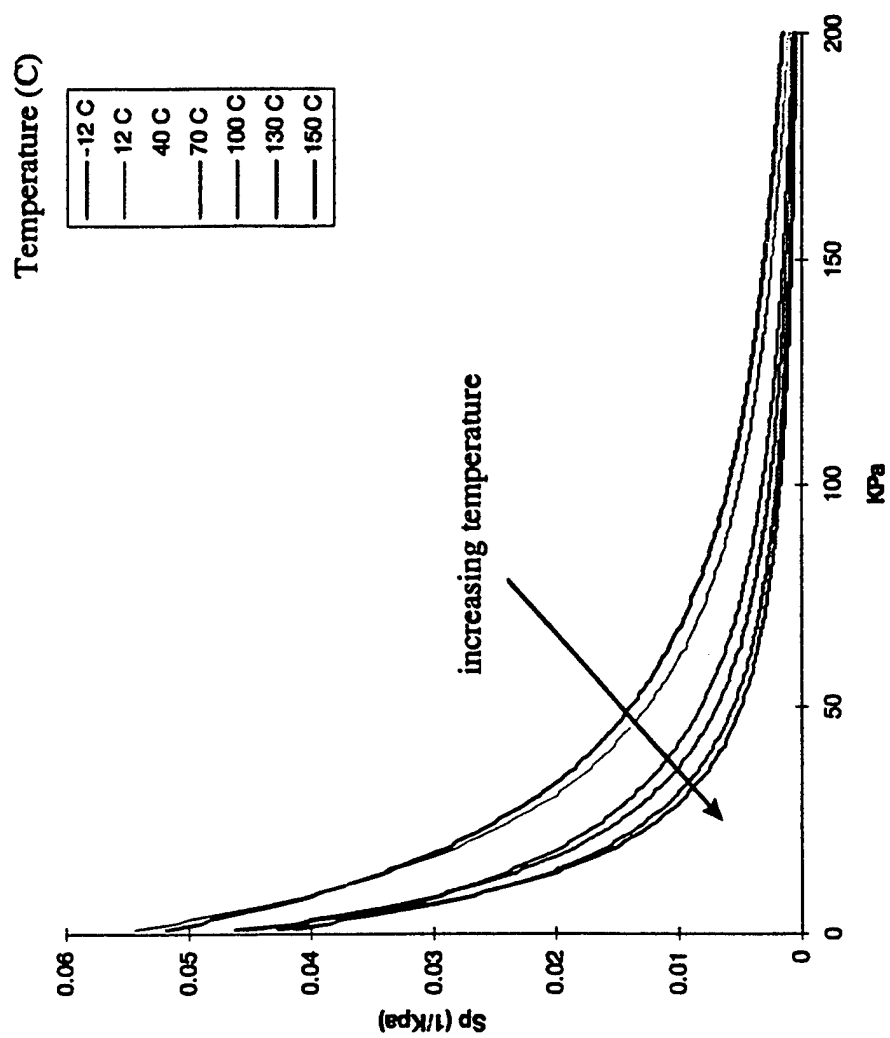


Figure 7.3 PSP sensitivity to pressure.

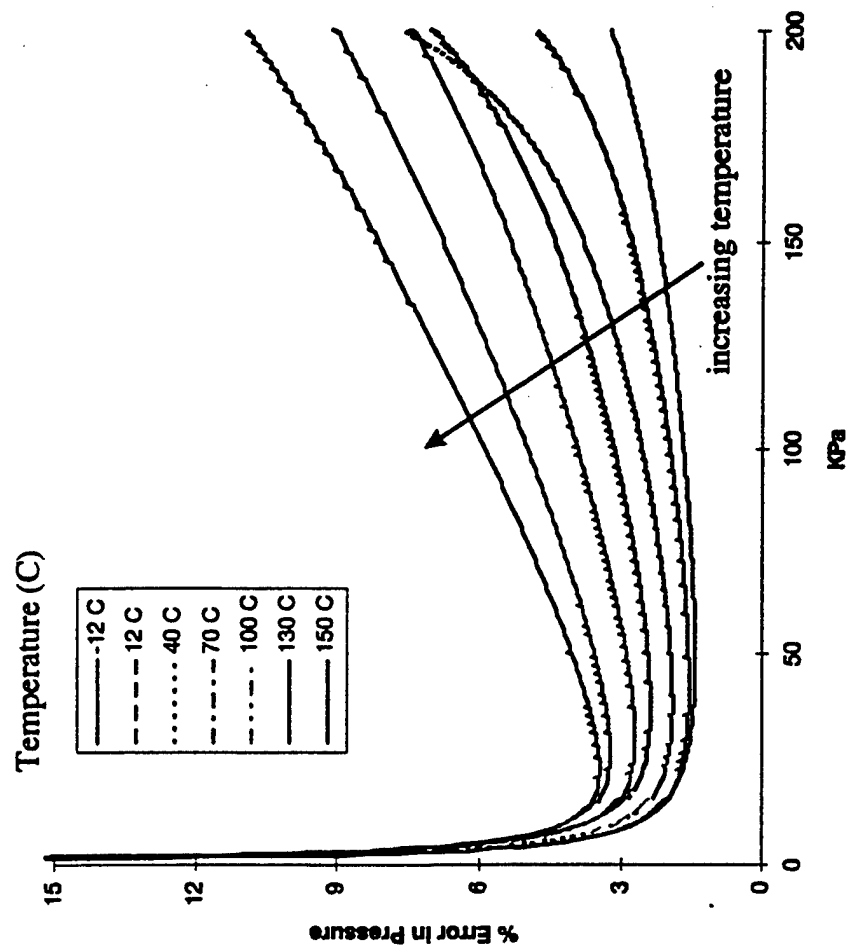


Figure 7.4 PSP percent error in pressure measurement as a function of pressure.



combinations from 10°C/60 kPa to 150°C/200 kPa are expected, corresponding to PSP sensitivities ranging from 0.010 - 0.00046 kPa<sup>-1</sup> and errors in pressure ranging from 0.96 - 22 kPa and TSP sensitivities ranging from ~0.0018 - ~0.007 T<sup>-1</sup> and errors in temperature ranging from ~1.73 - ~4.16°C. These errors can only be reduced by decreasing the uncertainty of the measured emittance (camera noise) or by increasing the fluorescence signal of the paints. The Stern-Volmer calibration results of the TSP and PSP data are presented in Appendix C along with the sensitivity and error calculations.

### **7.3 Effect of Oil On Paint Performance**

Because of the complexity of full-scale test facilities such as the CRF, “non-ideal” testing conditions are often encountered. For example, oil residue is a common occurrence in a compressor test. This is potentially a major problem for PSP and TSP measurements because most oils fluoresce. Since oil changes the reference intensity of the painted surface, pre-test wind-off images used in post-processing are invalidated. In a worst-case scenario, the oil could hinder the permeation of oxygen through the surface, inhibiting the pressure-sensing capability of the paint. Thus, it was important to investigate the effects of oil on the paint surface.

A simple experiment was conducted using the calibration chamber to view the effect of oil on the PSP. Figure 7.5 shows three calibrations of the same paint sample. First a fresh, clean sample was calibrated. The sample was then splattered with oil and re-calibrated. Finally, the sample was rinsed with alcohol to demonstrate a potential cleaning method and calibrated a third time. The oil and alcohol were applied in the

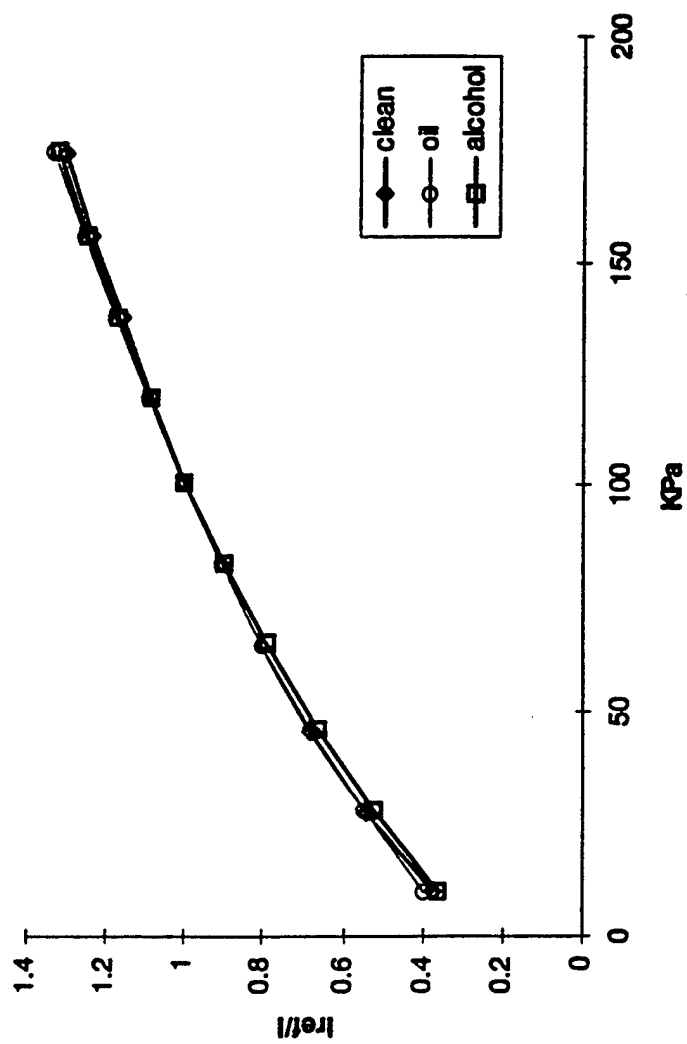


Figure 7.5 Effect of oil on PSP performance.

manner expected in the actual compressor test. The maximum change of 6% occurred at only 10 kPa. In the region of interest (30 - 200 kPa), the change ranged from 1.5 to 2%, and the overall pressure sensitivity appeared to be maintained. Attempts at cleaning the surface resulted in the recovery of only the low-end pressure sensitivity. Therefore, the added complexity of developing an on-line cleaning system was not deemed worthwhile. However, since the oil contamination normally occurs during the start-up procedure, it was recommended that the wind-off reference images be taken after data acquisition.

## **8.0 APPLICATION TO A TRANSONIC ROTOR**

For demonstration of the application, the selected pressure-sensitive paints were applied to a state-of-the-art transonic compressor. The compressor test was conducted during the period September 1996 to January 1997 at CRF. A detailed description of the CRF is given in Appendix D. The primary objective of this test was to obtain quantitative pressure measurements from the suction surface of the first-stage rotor. The following paragraphs present a general description of the test-article, the painting procedure, the test setup, and data-acquisition and post processing procedures.

### **8.1 Test-Article Description/Preparation**

The test article was the two-stage low-aspect-ratio transonic compressor shown schematically in Fig. 8.1. This compressor has been tested several times at the CRF; therefore, a large volume of data is available such as laser-Doppler-velocimeter (LDV),

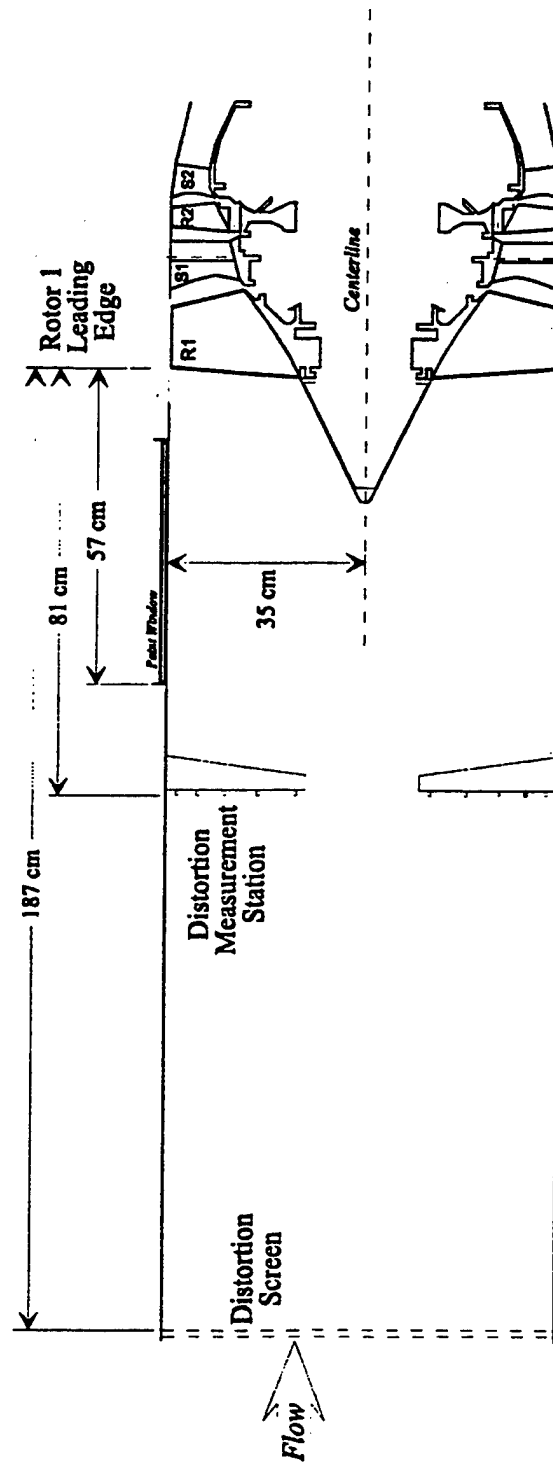


Figure 8.1 Test-article schematic.

distortion, and pressure-transducer results (37,39,40). The first-stage-rotor design parameters were previously presented in Table 5.1, and the CFD prediction was presented in Fig. 5.1. Rotor 1 airfoil-geometry parameters are presented in Table 8.1 (37).

Test-facility time constraints made it necessary to paint the rotor in place. The casing was removed prior to painting to allow better access. The instrumented blades were masked off for added protection. The blades were prepared by wiping them with a lint-free cloth using acetone; a clear primer coat was then applied and allowed to dry for a minimum of 6 hr to ensure adhesion of the paint to the blade. Fresh paint solutions were then mixed and applied to the blades using a commercial-artist air brush. Both the temperature and pressure paints were dry to the touch in  $\sim 1$  hr, but an 8 hr curing time was required. Figure 8.2 shows the painted blades.

Extreme caution was taken to minimize the exposure of the paint to room light. Pressure-sensitive paints display a common characteristic referred to as photo-degradation, whereby the paint-intensity signal deteriorates as a function of time with continued exposure of the paint to light. The painted blades could be used in up to four consecutive nights of testing if they were sufficiently covered during the day when repairs were being made to the test article. The painted blades were never tested for more than four consecutive nights since the facility was not in operation during weekends, allowing the opportunity to apply fresh paint. Advantage was taken of every opportunity to repaint since in the real-world test environment, the blade surfaces often collect dirt despite the 5- $\mu$  filters used to clean the air entering the CRF plenum.

**Table 8.1** Airfoil-geometry parameters for Rotor 1.

Parameter	Value
Number of Blades	16
Average Aspect Ratio	1.22
Inlet Radius Ratio	0.33
Average Radius Ratio	0.47
Tip Solidity	1.5
Max. Thickness/Chord	0.028

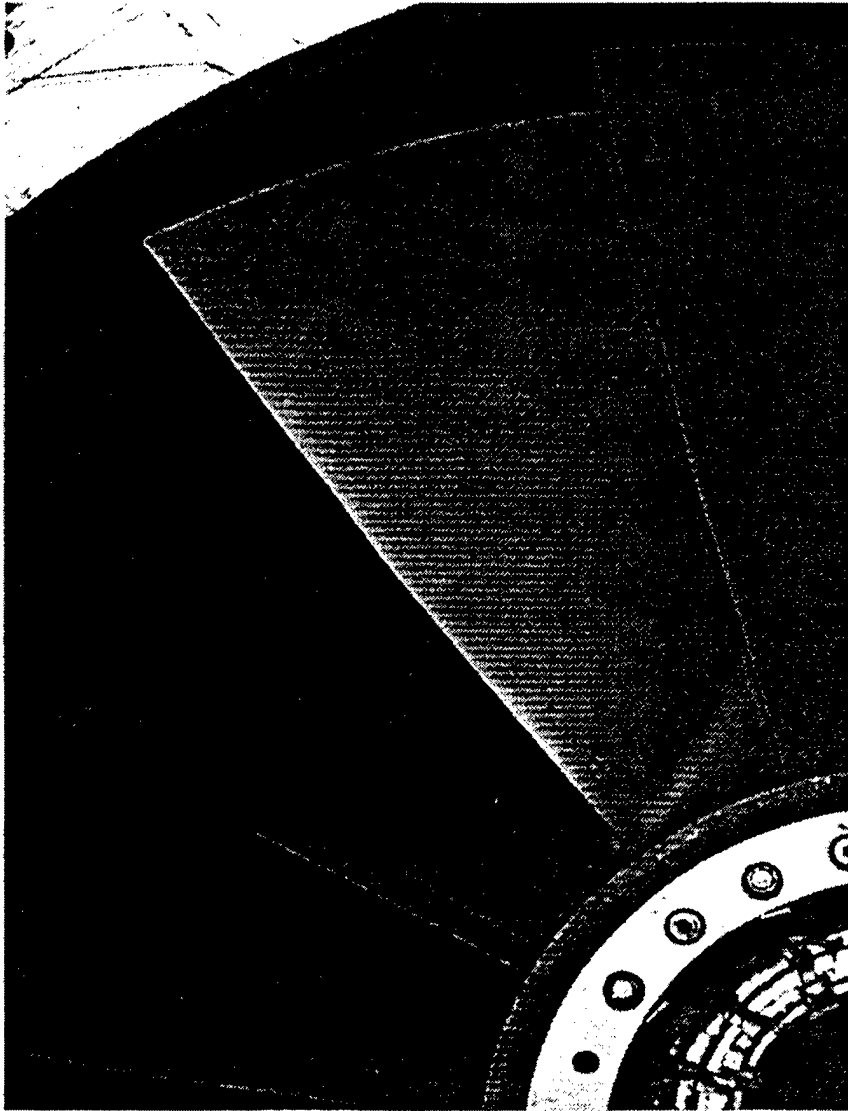


**Figure 8.2** Photograph of painted transonic-compressor blade.

After 1 hr of drying time, the alignment marks (traditionally black spots) were applied to the painted blades to provide regions of zero intensity in the data images. These marks play an important role in post-processing where they are used to align the wind-off and wind-on images. This is especially important in turbomachinery applications because of the twisting which occurs in a blade between quiescent and rotating conditions. In previous paint tests, as reported in Appendix A, quantitative measurement data were not obtained, primarily because of the inadequate alignment of these images.

Three alignment-mark requirements were identified. First, twelve or more consistent, uniformly distributed marks are necessary for successful warping of the twisted blade to permit its proper alignment with the reference image. Since these marks constitute regions where data are not collected, they should be as small as possible; however, they must be of sufficient size to be located in each image. Second, the marks should be in the same positions on each painted blade since a temperature-corrected pressure image can be obtained only if the temperature- and pressure-painted blades are aligned. Finally, the measured locations of the marks on the blades are also useful in determining the scale of the final images. For creating the alignment marks, a paper template was made of the blade surface; cuts were made to allow the paper to expand and follow the curve of the blade. With the template on the blade, a pencil, ruler, and piece of string were used to measure and indicate 33 alignment-mark positions. Holes ~ 1.6 mm in diameter were punched into the template at these locations. The template could easily



slide over the blade (with the case in place), and the marks were applied to the painted blades using a fine-point permanent marker.

Access to the test article was gained by removing the upstream ductwork, typically the Friday afternoon prior to a week of PSP testing. The primer coat was applied at this time and allowed to dry over the weekend. Since the CRF runs tests from 4 p.m. to midnight, the active paint layers were applied by 8 a.m. of the first test day to allow for the required 8 hr curing time. After a 1-hr drying time, the alignment marks were applied and the test-article ductwork was reassembled--usually by noon. The afternoon was then used to set up the data-acquisition equipment which is described in the following section.

## 8.2 Test Setup

The rotor test setup is shown in Fig. 8.3. A piece of duct upstream of the rotor was modified to accommodate a 330 x 25 mm window. A Princeton Instruments intensified CCD (ICCD) camera (576 x 384 pixels), fitted with a 50-mm f/1.2 lens, was located ~0.5 m upstream of the rotor at 90 deg (aft looking forward). The camera viewed the blades across the flow path and was angled ~5 deg below the centerline to avoid viewing the bullet nose. A 1-mJ nitrogen pulsed laser beam (337 nm, 200-ps pulse) was launched into a fiber which was mounted adjacent to the camera. The laser was used in the pulse-on-demand mode. The beam was expanded to illuminate the visible suction surface of the first-stage rotor. In this test setup the adjacent blade leading edge, coupled with the viewing angle, prevented viewing beyond 52% chord at the tip, and the image

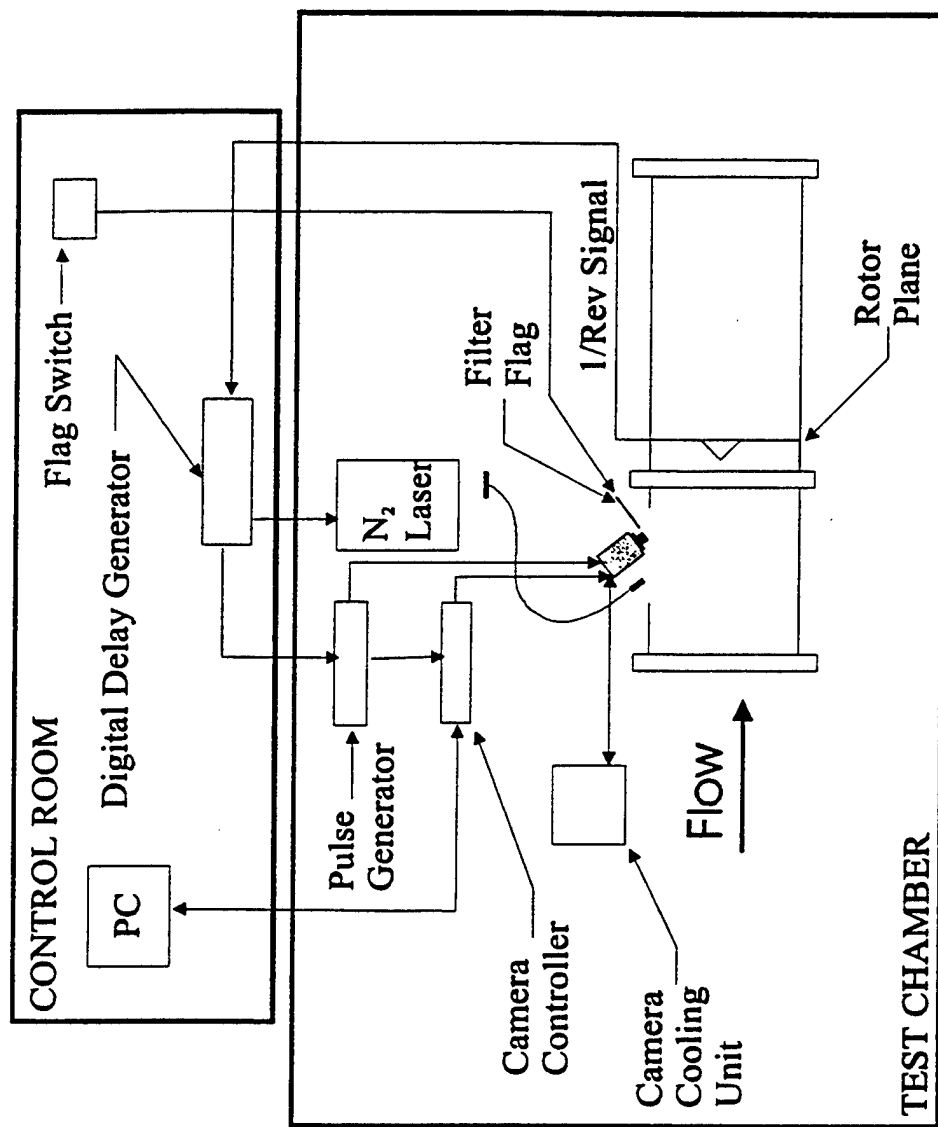


Figure 8.3 Transonic-rotor PSP test setup.

size restricted viewing beyond 62% span. For pressure and temperature measurements, ~61,500 pixels were focused on the blade. The detection system included the ICCD, an ST-138 camera controller for image acquisition and readout via the personal computer, and an FG-100 pulse generator for triggering the camera. The camera system and laser were mounted on an optical table inside the test chamber. A Neslab cooling unit was used to maintain the ICCD chip at  $-20^{\circ}\text{C}$  to minimize readout noise. The camera and nitrogen laser were remotely controlled from an adjacent room as a precaution. As mentioned previously, TSP requires a blue filter on the detector while PSP does not. For remote movement of the filter in and out of the measurement path, a magnetic flag was configured with a switch located in the control room. Figure 8.4 is a photograph of the described test setup.

The following procedure is used to stop blade motion and acquire data images. The operator sends the command to initiate image acquisition, the CCD camera is charged, and the 1/rev pulse is used to initiate the timing sequence. The 1/rev signal is delayed by the amount,  $\Delta t_{\text{delay}}$ , required to rotate the desired painted blade into the image plane. The delay generator sends out two pulses--the first to trigger the camera controller and the second to trigger the laser. The second pulse trails the first by  $13\text{ }\mu\text{s}$  to take into account the time required for the camera electronics to respond to the trigger. This allows synchronization of the arrival of the laser light at the blade surface and the activation of the camera intensifier for collecting the resulting fluorescence emission. The intensifier gain is typically set to 8. The period of operation of the intensifier (gate time) is



Figure 8.4 Photograph of the test setup.

determined by the laser pulse width and subsequent fluorescence emission of the paint. For this test a 200-ps laser pulse was used, and the maximum fluorescence lifetime was determined from calibration to be 323.5 ns (at vacuum and room temperature). The gate time was selected to be 10  $\mu$ s to take into account laser jitter on the order of 1  $\mu$ s. Therefore, the timing required to stop the blade motion ( $\sim$ 2  $\mu$ s) was achieved by the combination of the short laser pulse and the short-lived fluorescence of the paint--not by the gate of the intensifier. The camera "shutter," or charge time, was preset to a minimum of one rotor revolution. After the shutter closed, the acquisition of another image could not be initiated until the CCD downloaded the data to the computer. The readout time of the 221,184 pixel CCD chip was 234 ms.

### 8.3 Data-Acquisition Procedure

Four types of images are required in PSP and TSP measurements: a wind-off reference image, a wind-on test image, a black image, and a white image. The black images are taken with the lens cap on to define the thermal noise of the CCD array. The white image is taken of a uniformly lit surface using the same gate as the wind-on and wind-off images to provide a flat-field correction for the "honeycomb" pattern on the image that results from the minifier--the tapered fiber-optic coupling between the photocathode and the CCD chip. Both the black and white images are camera-dependent and can be taken either before or after the test. Thus, during a scheduled testing period, only the wind-off and wind-on images are acquired.

Wind-off images were acquired both before and after each night of testing to ensure that back-up reference images would be available for data processing if a failure occurred during the test. Also, these before and after wind-off images could be compared to determine whether oil was present in the compressor. For acquiring the wind-off images, the turning motor in the facility was used to rotate the rotor at a speed of 150 rpm. At this low speed the flow is negligible, providing valid reference images while allowing the timing circuitry to be used for accurate positioning of the blade images. For acquiring the wind-off images, the camera shutter was set to 400 ms. Sequential images were acquired using various delays until the desired painted blade appeared in the image. Care was taken to determine the delays required to place the TSP and PSP blades in the same location. The locations were determined by the pixel coordinates of the blade leading edge. The delay and coordinates of each blade were recorded. Twenty wind-off images were acquired for each paint for steady-state averaging. Once the wind-off images were acquired, the facility throttled the compressor to a desired test speed and condition. For the wind-on images, the camera shutter was reduced to 50 ms. To provide a constant background noise from image to image, the shutter value remained constant for all of the wind-on images, regardless of the rotational speed. From the coordinates previously recorded during the acquisition of the wind-off images, the delays required to superimpose the TSP and PSP blades were determined, and the corresponding wind-on images were acquired. A minimum of thirty wind-on images was acquired from each blade at each test condition for averaging to reduce random noise. No drift was apparent from shot to shot as a result ability of the CRF to maintain the rotor speed within 2-3 rpm.

#### 8.4 Post-Processing Procedure

The post-processing was carried out mainly by PAINTCP, a program developed for NASA Ames by Sterling Software, Inc (41). This package is used in PSP image analysis for wind tunnel aircraft model tests. For the purposes of this experiment, many of the functions within the code were not required; however, the program was used for its ability to register the alignment marks and align one image with another. First, PAINTCP reads all of the black, white, wind-off, and wind-on images for a given test condition. The 10 black, 20 wind-off, and 50 wind-on images are averaged. The images captured by the ICCD camera can be described as a product of camera sensitivity,  $S(x,y)$ , illumination power,  $P(x,y)$ , and the paint emission,  $E(x,y)$ , plus thermal background noise,  $B(x,y)$  as follows:

$$I(x,y) = S(x,y)P(x,y)E(x,y) + B(x,y) \quad (11)$$

where each parameter varies spatially. As a result of Eq. 11, two corrections must be made to the wind-off and wind-on images prior to division and conversion to quantitative temperature or pressure data: 1) a background correction to take into account the thermal noise on the ICCD chip, and 2) a flat-field correction to take into account the spatial variations in camera sensitivity and illumination (attenuation). The thermal noise can be easily removed by subtracting the background image, which only contains  $B(x,y)$ , from the wind-off and wind-on images. Removal of the camera attenuation is more difficult. A flat-field correction is used to remove the attenuation caused by the minifier--which results in a honeycomb pattern on the data image. This pattern--mechanical effect of the

camera--is fixed in all images; therefore, manipulation of the wind-on image to align it with the wind-off image will skew this pattern relative to the wind-on image, adding unnecessary noise to the final image, as illustrated in Fig. 8.5.

For removing the honeycomb pattern caused by the ICCD minifier, both the background-corrected wind-off and wind-on images are each divided by a white image--which is also background corrected. The process is depicted by equation 12

$$\begin{aligned}
 I_{x_{corrected}} &= \frac{I_x - I_{black}}{I_{white} - I_{black}} \\
 &= \frac{\{S(x,y)P(x,y)E(x,y) + B(x,y)\} - \{B(x,y)\}}{\{S(x,y)P(x,y)E_o(x,y) + B(x,y)\} - \{B(x,y)\}} = \frac{E(x,y)}{E_o(x,y)} \quad (12)
 \end{aligned}$$

where x represents either the wind-off or wind-on condition and the white image records the sensitivity, illumination power, and a reference emission,  $E_o(x,y)$ . All of the images (white, wind-off, and wind-on) are corrected for thermal noise,  $B(x,y)$ , by subtracting the background image,  $I_{black}$ . Dividing the wind-off and wind-on images by a white image effectively removes  $S(x,y)$  and  $P(x,y)$ , leaving only the ratio of the paint emission,  $E(x,y)$ , and the reference emission used to create the white image,  $E_o(x,y)$ . As mentioned in Section 8.3, the black image is obtained by acquiring an image with the lens cap on the camera ( $P = E = 0$ ), and the white image is obtained by acquiring an image from a uniformly lit flat surface. This procedure removes the thermal noise caused by the CCD



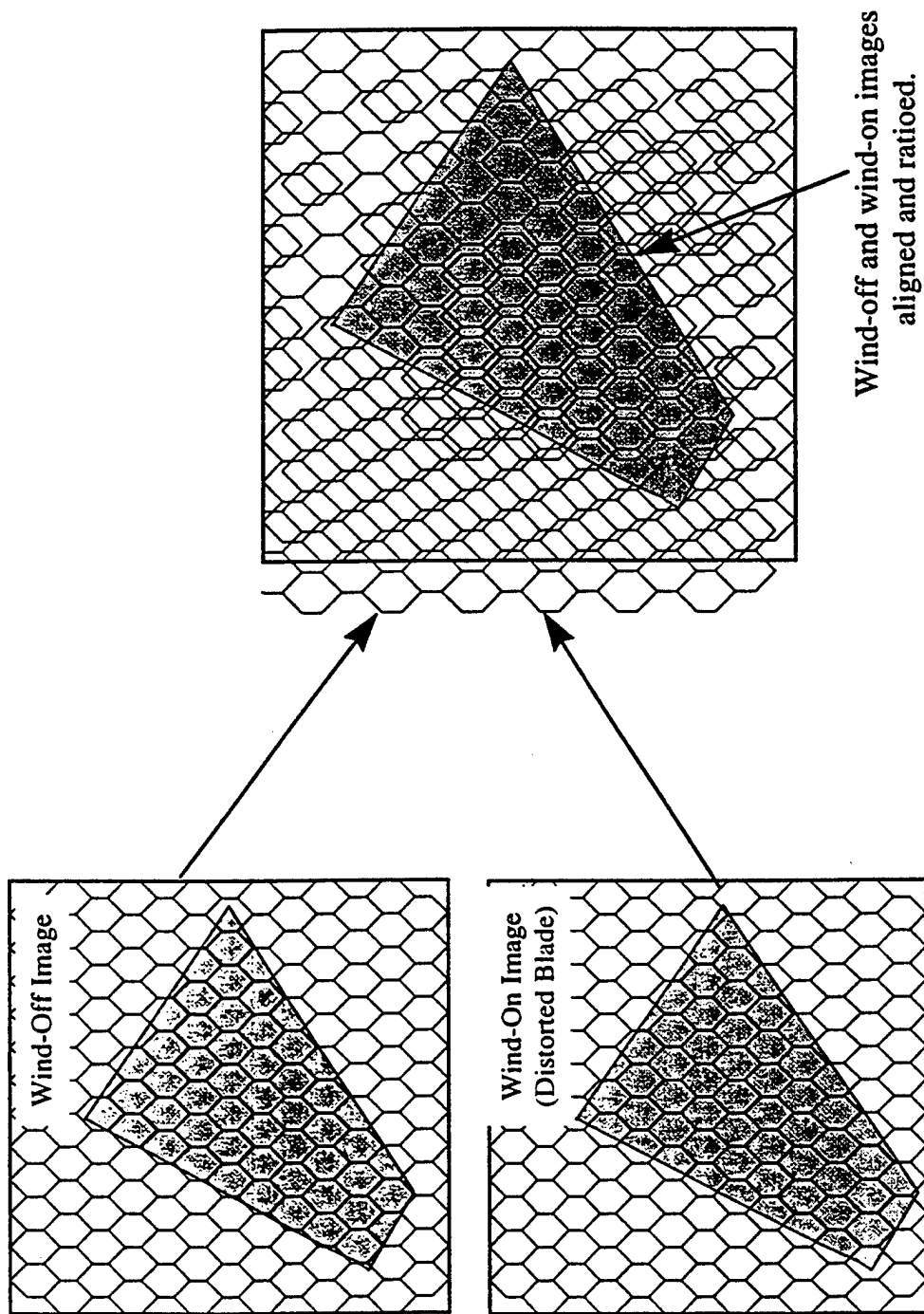


**Figure 8.5** Honeycomb-pattern noise caused by ICCD minifier.

and the honeycomb pattern caused by the fiber-optic coupler of the camera;  $E_o(x,y)$  cancels when the corrected wind-off image is divided by the corrected wind-on image.

Once the wind-off and wind-on images are corrected, the PAINTCP program locates the alignment marks on the corrected wind-on image and uses them to "warp" the image to match the pattern of alignment marks in the corrected wind-off image. The wind-off image is then divided by the properly aligned wind-on image, and this final-image ratio is written to an IEEE floating binary file. This procedure is performed twice for each test condition--once for the TSP data and once for the PSP data. In order to temperature-correct the PSP data, the TSP image must be aligned with the PSP image. Therefore, all of the pressure and temperature images are aligned to the same wind-off PSP image.

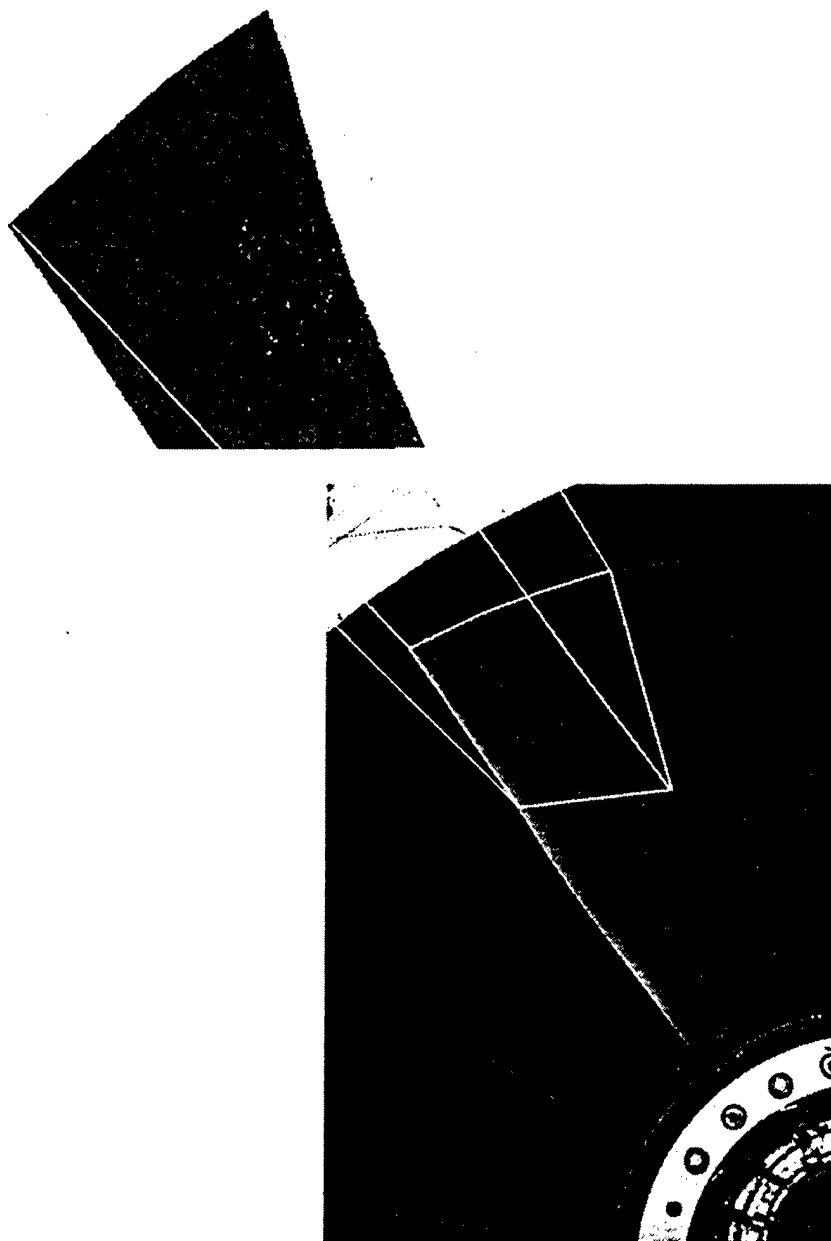
The output from the PAINTCP program is read into Transform, a software application which allows matrix and image manipulation. The equation determined from the Stern-Volmer calibration for the TSP is applied to the temperature matrix to convert the intensity ratio to surface temperatures (in °C). The results are output to a new matrix. Because the temperature image is aligned with the pressure image using PAINTCP, the temperature image can be used to calibrate the pressure image directly. The surface-temperature information and the intensity-ratio data from the PSP are input to the calibration equation for the PSP, and the resulting surface-pressure information is output to a new matrix. The final temperature image and temperature-corrected pressure image are scaled and plotted with false-color using the Transform software.

## 9.0 TRANSONIC-ROTOR TEST RESULTS

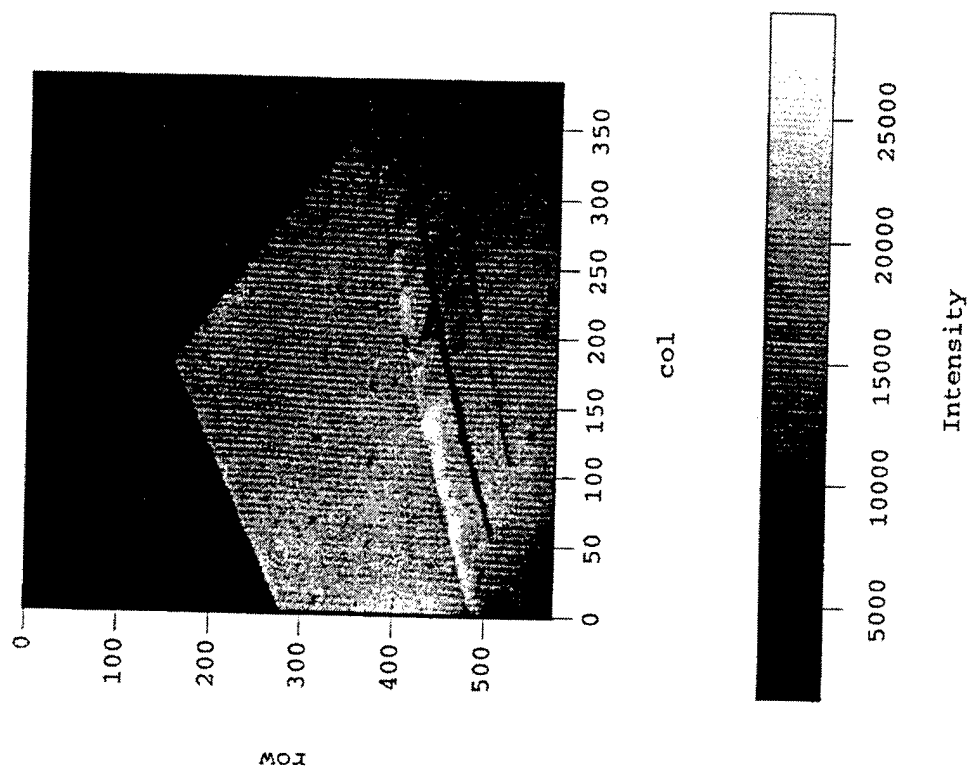
Data were acquired under various test conditions at corrected speeds ranging from 68 to 98.6%. More than 5 GB of data were acquired, most of which has not yet been processed. Only the preliminary data of the peak-efficiency (PE) condition at 85% corrected speed will be reported here.

Figure 9.1 depicts the area of the blade where temperature and pressure data were acquired. The approximate dimensions of the viewable area of the blade where data were acquired are from 0-52% chord at the tip and from 62-100% span at the leading edge. The raw PSP and TSP wind-on gray-scale images obtained at the 85%  $N_c$ , peak-efficiency condition are presented in Figs. 9.2 and 9.3, respectively. The blade-leading-edge tip is located in the upper-right corner and rotates counterclockwise for both images. Using the alignment marks in the images, the spatial resolution was determined to be 0.1575 mm for a total of 61,500 measurement points on the blade surface. The flat-field correction was not applied to Fig. 9.2; and the honeycomb pattern which results from the noise can be observed. As evident in Fig. 9.3, use of the flat-field image removes a large amount of the minifier noise; note the two tip shockwaves present in the TSP image.

Figures 9.4 and 9.5, respectively, present TSP and PSP results obtained using the post-processing procedure described above. A temperature range of  $-10 - +60^{\circ}\text{C}$  was quantified by the TSP in the measurement area (62 - 100% span at the leading edge, 0 - 52% chord at the tip). The TSP data are used to correct the PSP data, presented in Fig. 9.4 which reveals a pressure range of 20 -  $\sim 120$  kPa in the measurement area. These



**Figure 9.1** First-stage-rotor image region.



**Figure 9.2** PSP wind-on image , 85% Nc, peak-efficiency operating condition, displaying honeycomb-noise pattern.

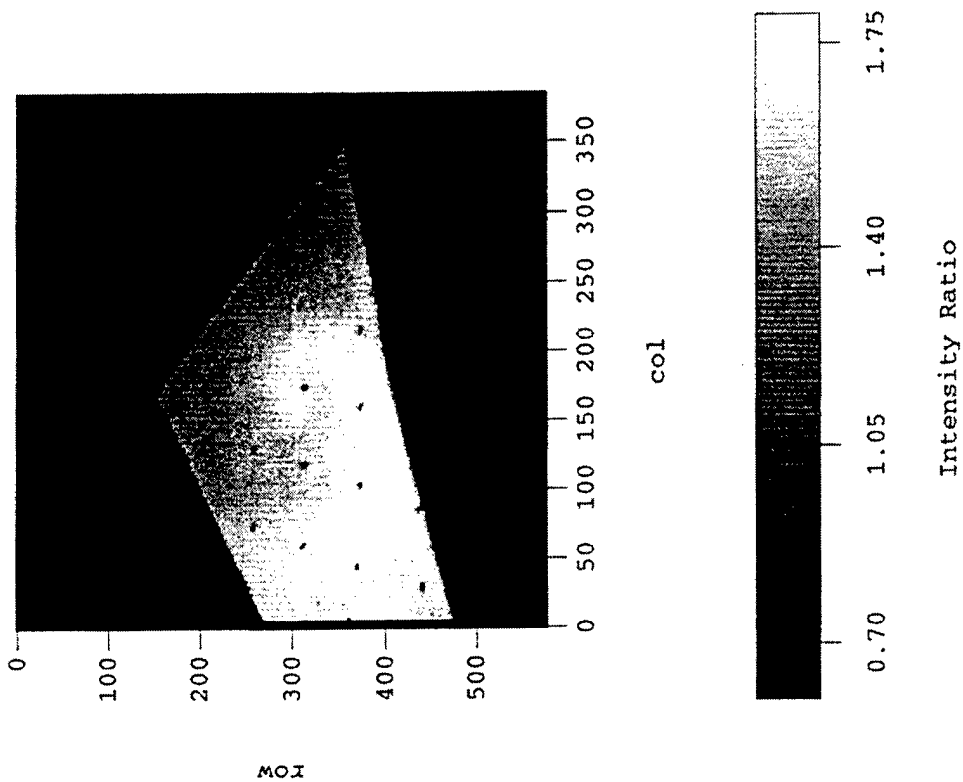


**Figure 9.3** Flat-field corrected TSP wind-on image, 85%  $N_c$ , peak-efficiency operating condition, displaying two visible shockwaves.

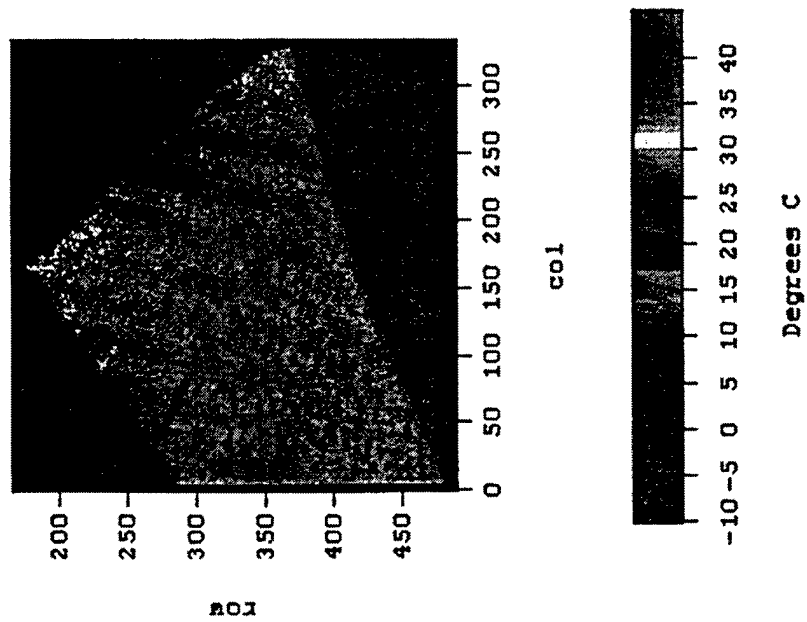
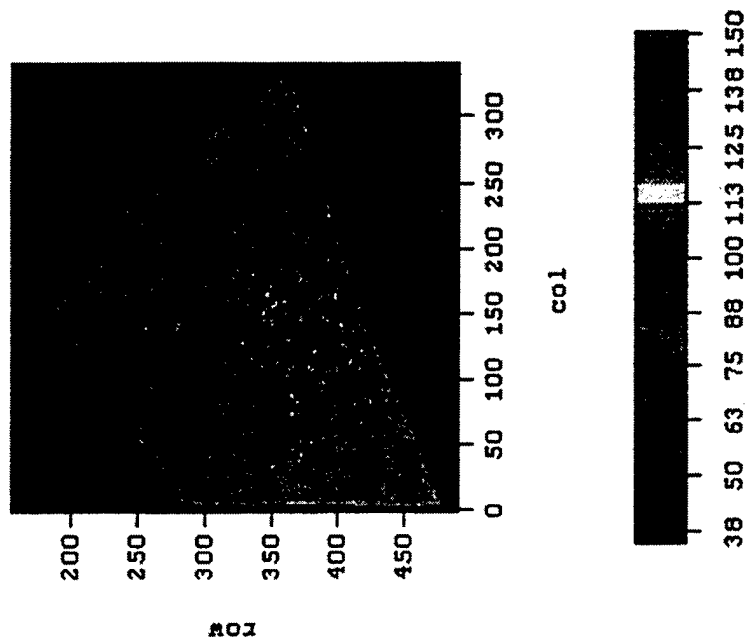


Figure 9.4 Calibrated TSP image at 85% Nc, peak-efficiency operating condition.



KPa (101.28 KPa = 1 atmosphere)

Figure 9.5 Calibrated temperature-corrected PSP image, 85% Nc, peak-efficiency operating condition.



pressure and temperature combinations correspond to estimates in temperature measurement error of 0.5 - 2.5°C and estimates in pressure-measurement error of 0.36 - 4 kPa (Appendix C).

Comparison of the clarity of the raw images and the final images indicates that the minifier attenuation was not sufficiently removed; the resulting noise level washes out the two shockwaves in the final TSP image. This is thought to be due to the non-uniform illumination of the paint blade. Unfortunately, in the compressor environment the lighting on the high-curvature blade is not uniform over the entire image; as a result, the use of a traditional white image of uniform intensity for flat-field correction does not remove the honeycomb pattern. Therefore, the final image still contains the mapping noise depicted in Fig. 8.5, even though the image presented in Fig. 9.3 appears to be flat-field corrected. The pattern noise is worse in the PSP data because the image combines the pattern noise from the TSP and the PSP images.

## 10.0 CONCLUSIONS

This thesis has described the photophysical properties of luminescent molecules which allows them to be used as pressure-sensing devices. PSP performance requirements for turbomachinery applications have been identified and fluorescence determined to be the appropriate luminescent process for turbomachinery applications based upon the timing required to stop the rotating image. Development and calibration of fluorescence-based PSPs and TSPs capable of performance up to 2 atm and 150 °C have been detailed. The painting procedure, test setup, data acquisition, and post-

processing procedures have been presented. The preliminary TSP and PSP data acquired from the suction surface of a transonic rotor at 85% corrected speed under the peak-efficiency condition have been presented. Visual comparison of the final PSP image presented in Fig. 9.5 and the CFD prediction presented earlier in Fig. 5.1 reveal the same pressure trends. Efforts are underway to recreate the test setup and acquire the proper white image (with non-uniform illumination) required to eliminate the honeycomb pattern. Once the final images are obtained measurement errors will be assessed and compared to the predicted values.

Overall, this thesis has demonstrated the potential of using the PSP technique for applications in advanced turbomachinery. Several areas must be improved to bring this technology to fruition. First, improved methods of applying the alignment marks required for post-processing must be developed. The current method of application is very difficult and, as a result, the probability of accurate placement is low. The new technique should be simple and provide precise placement of consistent alignment marks with known three-dimensional coordinates to provide a means of correlating the two-dimensional PSP image and the three-dimensional blade geometry.

Second, the noise resulting from the ICCD minifier must be eliminated during post-processing. This can be accomplished simply through the use of an alternative detection device that does not utilize fiber-optic coupling between the photocathode and the CCD chip or through the use of a reference paint. Alternative cameras are currently being evaluated; in the meantime, a reference paint will be developed. A reference paint is basically a fluorescent paint which is neither temperature nor pressure sensitive and, as a result, will indicate the illumination power over the surface. For future tests if an improved camera is not yet available, three separate blades will be painted for independent temperature, pressure, and reference (power) measurements.

Finally, paint-development efforts must continue on improving pressure sensitivity and achieving higher pressure and temperature capability higher to accommodate later fan stages. Improvements in pressure sensitivity will rely on the development of probe molecules with improved quantum efficiencies (QE)--which will increase the SNR. PSP developers are constantly seeking new probes with higher QEs because every PSP application can benefit from increased luminescent signals. Unfortunately, most current PSP research is based upon the use of organic probe molecules. The prominence of organic-based PSPs is largely historical, building on its initial developments in the field; however, the organic molecules traditionally used for PSPs (porphyrins) are not the optimal lumiphores for PSP measurements. Organic molecules are problematic in that they are temperature- and photo-sensitive and are inefficient oxygen quenchers; they also have an upper temperature limit on the order of 200°C.

Evolving PSP technology is now facing difficult challenges and will not experience the degree of progress that it has in the past. It will become increasingly difficult to deliver the sensitivity and accuracy that researchers demand using off-the-shelf probe molecules and binding systems. For these reasons, future research efforts will be focused on the development of an all-inorganic PSP. Through the synthesis of probe molecules, scientists can control the mechanisms which determine the temperature and pressure capability as well as the pressure sensitivity of PSP technology. With some inorganic salts having the capability to perform up 1000°C, inorganic oxygen sensors hold the most promise for the successful development of a PSP for later compressor stages.

## REFERENCES

- (1) Peterson, J. I., and Fitzgerald, V. F., "New Technique of Surface Flow Visualization Based on Oxygen Quenching of Fluorescence," *Rev. Sci. Instrum.*, Vol. 51, No. 5, pp. 670-671, 1980.
- (2) Bukov, A. P., Orlov, A. A., Mosharov, V. E., Radchenko, V. N., Pesetsky, V. A., Sorokin, A. V., Phonov, S. D., Alaty, L., and Colucci, V., "Application of Luminescent Quenching for Pressure Field Measurements on the Model Surface in a Wind Tunnel," *Wind Tunnels and Wind Tunnel Test Techniques*, The Royal Aeronautical Society, Southampton University, United Kingdom, September 1992.
- (3) Bukov, A., Mosharov, V., Orlov, A., Pesetsky, V., Radchenko, V., Phonov, S., Matyash, S., Kuzmin, M., and Sadozsky, N., "Optical Surface Pressure Measurements: Accuracy and Application Field Evaluation," 73rd AGARD Fluid Dynamics Panel Meeting and Symposium on Wall Interference, Support Interference, and Flow Field Measurements, Brussels, Belgium, 1993.
- (4) Troyanovsky, I., Sadocskii, N., Kuzmin, M., Mosharov, V., Orlov, A., Radchenko, V., and Phonov, S., "Set of Luminescence Pressure-Sensors for Aerospace Research," *Sens. and Act.*, Vol. 11, pp. 201-206, 1993.
- (5) Ardasheva, M. M., Nevskii, L. B., and Pervushin, G. E., "Measurement of Pressure Distribution by Means of Indicator Coatings," *J. Appl. Mech. Tech. Phys.*, No. 4, pp. 24-33, 1985.
- (6) Volan, A., and Alafi, L., "New Optical Pressure Measurement System," IEEE 14th International Congress of Instrumentation in Aerodynamic Simulation Facilities (ICIASF), New York, 1991, pp. 10-16.

- (7) Engler, R. H., Hartmann, K., and Schultze, B., "Aerodynamic Assessment of a New Optical Pressure Measurement System (OPMS) by Comparison with Conventional Pressure Measurements in a High Speed Wind Tunnel," IEEE 14th International Congress of Instrumentation in Aerodynamic Simulation Facilities (ICIASF), New York, 1991, pp. 17-24.
- (8) Engler, R. H., "Further Developments of Pressure Sensitive Paint (OPMS) for Non-Flat Models in Steady Transonic Flow and Unsteady Conditions," CH34827-95, IEEE 16th International Congress on Instrumentation in Aerospace Simulation Facilities (ICIASF), Wright-Patterson AFB, OH, 1995, pp. 33.1-8.
- (9) "Luminescent Pressure Sensors (LPS) and Luminescent Pressure Sensitive Paints (PSP)," *OPTROD Ltd.*, Dugin str. 17-31, Zhukovsky, Moscow reg., 140160 Russia, 1995.
- (10) Bykov, A., Fonov, S., Kishalov, A., Mosharov, V., Orlov, A., Ostroukhov, S., and Radchenko, V., "Application of Luminescent Pressure Sensor Technology to Propellers," Central Aero-Hydrodynamic Institute Internal Document, Preprint No. 99, Moscow, 1995.
- (11) Davies, A. G., Bedwell, D., Dunleavy, M., and Brownjohn, N., "Pressure Sensitive Paint Measurements Using Phosphorescence Lifetime Method," 7th International Symposium on Flow Visualization, Seattle, WA, 1995.
- (12) Sant, Y. L., and Mérienne, M. C., "An Image Resection Method Applied to Mapping Techniques," CH34827-95, IEEE 16th International Congress on Instrumentation in Aerospace Simulation Facilities (ICIASF), Wright-Patterson AFB, OH, 1995, pp. 46.1-8.

- (13) Gouterman, M., Callis, J., Burns, D., Kavandi, J., Gallery, J., Khalil, G., Green, E., McLachlan, B., and Crowder, J., "Luminescence Imaging for Aerodynamic Testing," ONR/NASA Workshop on Quantitative Flow Visualization, J. Sullivan and B. Holmes (eds.), Purdue University, West Lafayette, IN, 1990.
- (14) Kavandi, J., Callis, J., Gouterman, M., Khalil, G., Wright, D., Green, E., Burns, D., and McLachlan, B., "Luminescent Barometry in Wind Tunnels," *Rev. Sci. Instrum.*, Vol. 61, No. 11, pp. 3340-3347, 1990.
- (15) McLachlan, B. G., Bell, J. H., Kennelly, R. A., Schreiner, J. A., Smith, S. C., and Strong, J. M., "Pressure-Sensitive Paint Use in the Supersonic High-Sweep Oblique Wing (SHOW) Test," AIAA-92-2686, AIAA 10th Applied Aerodynamics Conference, Palo Alto, CA, 1992.
- (16) McLachlan, B. G., J. H. Bell, J. Gallery, M. Gouterman, and J. Callis, "Boundary Layer Transition Detection by Luminescence Imaging," AIAA Paper No. 93-0177, AIAA 31st Aerospace Sciences Meeting and Exhibit, Reno, NV, 1993.
- (17) Harris, J., and Gouterman, M., "Referenced Pressure Sensitive Paint for Flow Visualization VII," 7th International Symposium on Flow Visualization, Seattle, WA, 1995.
- (18) McLachlan, B. G., and Bell, J. H., "Pressure-Sensitive Paint in Aerodynamic Testing," *Exp. Thermal Fluid Sci.*, Vol. 10, pp. 470-485, 1995.
- (19) Crites, R. C., Benne, M. E., Morris, M. J., and Donovan, J. F., "Optical Surface Pressure Measurements: Initial Experience in the MCAIR PSTWT," Wind Tunnels and Wind Tunnel Test Techniques, The Royal Aeronautical Society, Southampton University, United Kingdom, 1992.

- (20) "Pressure-Sensitive Paint: A New Development Tool," *MCAIR Digest*, Vol. 29, No. 3, 1992.
- (21) Morris, M. J., "Use of Pressure-Sensitive Paints in Low Speed Flows," CH34827-95, IEEE 16th International Congress on Instrumentation in Aerospace Simulation Facilities (ICIASF), Wright-Patterson AFB, OH, 1995, pp.31.1-10.
- (22) Hamner, M., B. Campbell, T. Liu, and J. Sullivan, "A Scanning Laser System for Temperature and Pressure-Sensitive Paint," AIAA- Paper No. 94-0728, AIAA 32nd Aerospace Sciences Meeting and Exhibit, Reno, NV, 1994.
- (23) Burns, S., and Sullivan, J., "The Use of Pressure Sensitive Paint on Rotating Machinery," CH34827-95, IEEE 16th International Congress on Instrumentation in Aerospace Simulation Facilities (ICIASF), Wright-Patterson AFB, OH, 1995, pp.32.1-14.
- (24) Liu, T., Johnston, R., Torgerson, S., Fleeter, S., and Sullivan, J., "Rotor Blade Pressure Measurement in a High Speed Axial Compressor using Pressure and Temperature Sensitive Paints," AIAA Paper No. 97-0162, AIAA 35th Aerospace Sciences Meeting and Exhibit, Reno, NV, 1997.
- (25) Jagharhi, A. J., Mitchell, M., Burkett, C., and Sealey, S., "Wind Tunnel Application of Pressure Sensitive Paints at NASA Langley Research Center (8 foot TPT & 7'x10' HST)," NASA LaRC IRD ATMB, NASA Langley Research Center, Hampton, VA, 1993.
- (26) Oglesby, D. M., Leighty, B. D., and Upchurch, B. T., "Pressure Sensitive Paint with an Internal Reference Luminophore," 41<sup>st</sup> International Instrumentation Symposium, Instrument Society of America, Denver, CO, 1995, pp. 381-395.

- (27) Oglesby, D. M., Upchurch, B. T., Leighty, B. D., and Simmons, K. A., "Pressure Sensitive Paint with Internal Temperature Sensing Lumiphore," 42nd International Instrumentation Symposium, Instrument Society of America, San Diego, CA, 1996.
- (28) Carroll, B. F., Winslow, A., Abbitt, J., Schanze, K., and Morris, M. M., "Pressure Sensitive Paint: Application to a Sinusoidal Pressure Fluctuation CH34827-95, IEEE 16th International Congress on Instrumentation in Aerospace Simulation Facilities (ICIASF), Wright-Patterson AFB, OH, 1995, pp. 35.1-6.
- (29) Hubner, J. P., Abbitt, J. D., and Carroll, B. F., "Pressure Measurements on Rotating Machinery using Lifetime Imaging of Pressure Sensitive Paint," AIAA Paper No. 96-2934, 32nd AIAA/ASME/SAE/ASEE Joint Propulsion Conference and Exhibit, Orlando, FL, 1996.
- (30) Sellers, M. E., and J. A. Brill, "Demonstration Test of Pressure-Sensitive Paint in the AEDC 16 ft Transonic Wind Tunnel Using the TST Model," AIAA Paper No. 94-2481, AIAA 18th Aerospace Ground Testing Conference, Colorado Springs, CO, 1994.
- (31) Sabroske, K. R., Rabe, D. C., and Williams, C., "Pressure-Sensitive Paint Investigation for Application in Turbomachinery," ASME Paper No. 95-GT-92, ASME International Gas Turbine and Aeroengine Congress and Exposition, Houston, Texas, 1995.
- (32) Bencic, T., "Experiences Using Pressure-Sensitive Paint in NASA Lewis Research Center Propulsion Test Facilities," AIAA Paper No. 95-2831, 31st AIAA/ASME/SAE/ASEE Joint Propulsion Conference and Exhibit, San Diego, CA, 1995.



- (33) Kautsky, H., "Quenching of Luminescence by Oxygen," Trans. of the Faraday Society, No. 35, 1939, pp. 216.
- (34) Ingle, J. D. Jr., and Crouch, S. R., *Spectrochemical Analysis*, Prentice Hall, New Jersey, Ch. 12, 1988, pp. 338-351.
- (35) Russler, P., Rabe, D., Cybyk, B., and Hah, C., "Tip Flow Fields in a Low Aspect Ratio Transonic Compressor," ASME Paper No. 95-GT-089, ASME International Gas Turbine and Aeroengine Congress and Exposition, Houston, Texas, 1995.
- (36) Copenhaver, W. W., Hah, C., and Puterbaugh, S. L., "Three-Dimensional Flow Phenomena in a Transonic, High-Through-Flow, Axial-Flow Compressor Stage," *J. Turbomachinery*, Vol. 115, No. 2, pp. 240-248, 1993.
- (37) Russler, P., "Acquisition and Reduction of Rotor Tip Static Pressure Transducer Data From a Low Aspect Ratio Transonic Fan," Wright Laboratory Technical Report WL-TR-95-2022, Wright Laboratory, Wright-Patterson Air Force Base, OH, 1995.
- (38) Rabe, D., Bölcs, A., and Russler, P., "Influence of Inlet Distortion on Transonic Compressor Blade Loading," AIAA Paper No. 95-2461, 31st AIAA/ASME/SAE/ASEE Joint Propulsion Conference and Exhibit, San Diego, CA, 1995.
- (39) Torgerson, S., Liu, T., and Sullivan, J., "Use of Pressure-Sensitive Paints in Low-Speed Flows," 19th AIAA Advanced Measurement and Ground Testing Technology Conference, New Orleans, LA, 1995.

(40) Oglesby, D. M., Puram, C. K., Upchurch, B. T., "Optimization of Measurements with Pressure Sensitive Paints," NASA Technical Memorandum 4695, NASA Langley Research Center, Hampton, VA, 1995.

(41) *PaintCp V2.2 User's Guide*, Sterling Software Technical Note TN-93-8006-000-48, 1994.

## APPENDIX A: Previous PSP Experiences in Turbomachinery

A low-speed demonstration of PSP data acquisition was conducted in August of 1994 at the Wright Laboratory Compressor Research Facility (CRF). Qualitative data were acquired from the suction surface of a subsonic high-aspect-ratio fan blade. The intensity-based method was used in conjunction with an optical derotation device for stopping the rotating image. The details of the experimental test setup and the optical derotator can be found in reference 32. Figure A.1 shows the wind-on image acquired from the fan rotating at 1,500 rpm. The CCD camera and lens system allowed ~10,000 measurement points on the blade surface. Each pixel measured the light intensity reflected from the blade and represented a potential pressure-measurement location on this blade during rotation. In the figure the hub is located at the top left and the tip of the blade, at the lower right. The direction of rotation is clockwise in this view. The light areas correspond to the highest intensities (low pressures) and the dark areas, to the lowest intensities (high pressures). This trend in intensity can be seen more clearly in the chord-wise plot of the blade shown in Fig. A.2; the black line in Fig. A.1 indicates the location of the slice. If one remembers that the pressure is inversely related to the intensity, Fig. A.2 clearly shows that the pressure at first decreases and then increases along the chordline, as expected on the suction surface of a subsonic airfoil. Paint developed by Arnold Engineering and Development Center (AEDC) was used in this experiment. Quantification of these data was not possible because the wind-off and wind-on images could not be sufficiently aligned during post-processing.

A follow-on experiment was conducted at the CRF on a full-scale transonic rotor in March of 1996. The technique employed in the low-speed demonstration was used;

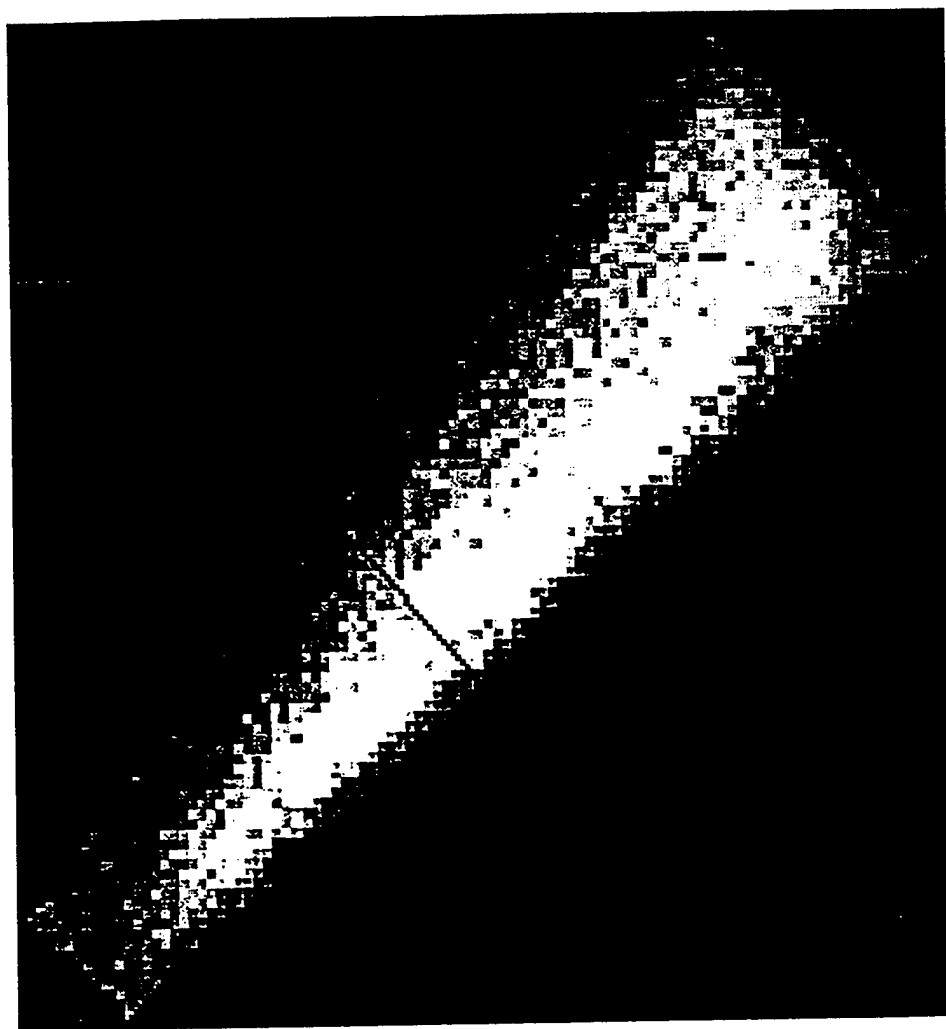


**Figure A.1** Wind-on intensity measurement at 1,500 rpm.

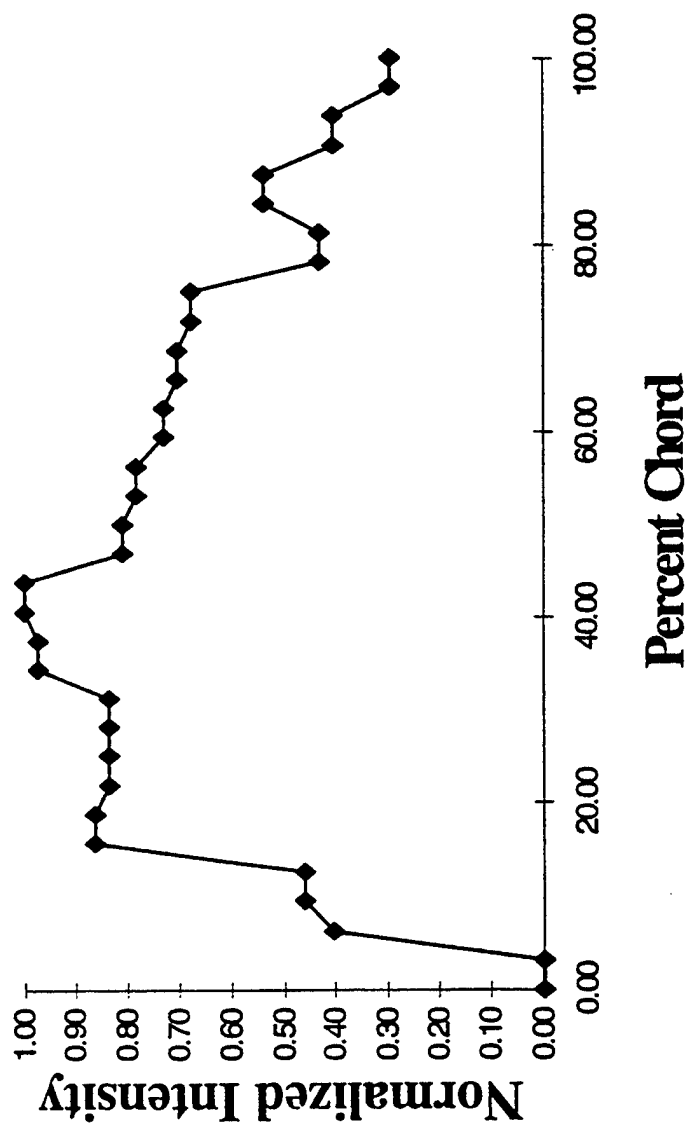
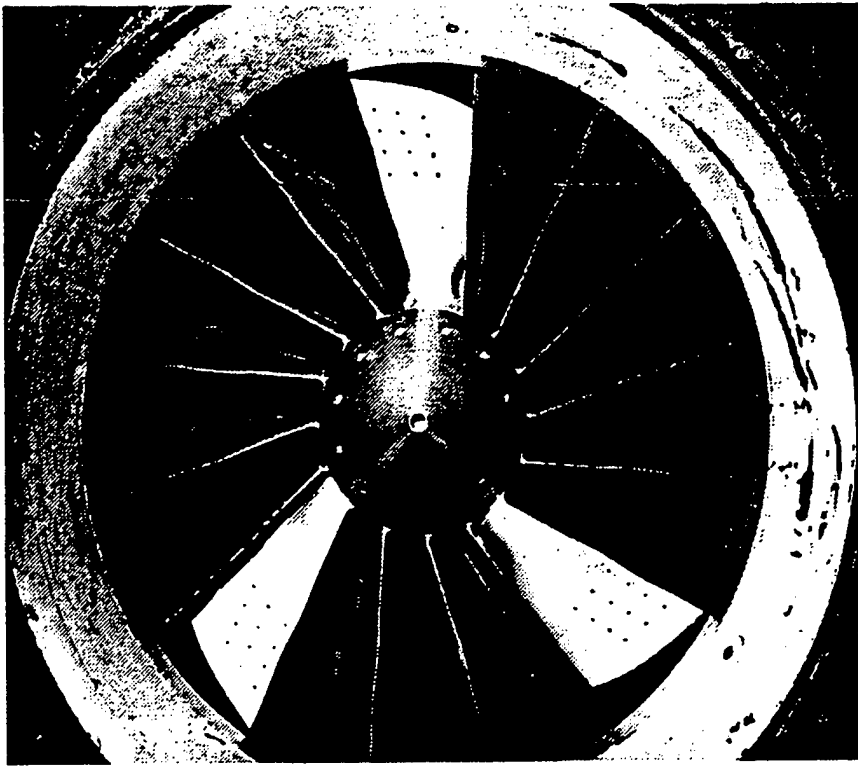


Figure A.2 Plot of normalized intensity vs. percent chord on the suction surface.

however, a gated, intensified CCD (ICCD) camera and pulsed laser were used to stop the blade motion; the paint was obtained from the Central Aero-Hydrodynamics Institute in Moscow (TsAGI). In this test a small (2.5- $\mu$ J) pulsed nitrogen laser was expanded to illuminate the blade surface for exciting the paint. The once-per-revolution signal triggered both the laser and the camera. The timing requirement for stopping the blade motion, calculated in Appendix B, was determined to be an  $\sim$ 2- $\mu$ s window. Thus, a paint with a fast luminescent-decay time, or fluorescent paint, would be needed. Unfortunately, most of the paints (including the AEDC paint used in the previous rotor experiment) available at that time utilized the slower phosphorescent process to optimize pressure sensitivity. The only fluorescent paint available was the LPS-2 made by TsAGI.

Figure A.3 shows the painted blades of the test article. The laser and ICCD camera shared a common access port, located 2 ft upstream of the rotor at -10 deg off top dead center. The port was 12.7 mm wide and 50.8 mm long. The camera imaged the blade across the bullet nose in the lower right quadrant. The TsAGI paint employs the aromatic fluorophore pyrene and is described in reference 9. Although the paint adhered to the blade and provided a sufficient signal for data acquisition, it lacked the pressure sensitivity required for adequate resolution of the blade flow phenomena. For this reason only a faint step change across the shock could be resolved, as seen in Fig. A.4. The flow condition in the figure was 85%  $N_c$  at the peak-efficiency condition. Again, quantification of the data was not possible because the wind-off and wind-on images could not be properly aligned.



**Figure A.3** Painted blades of test article used in preliminary transonic-rotor test.

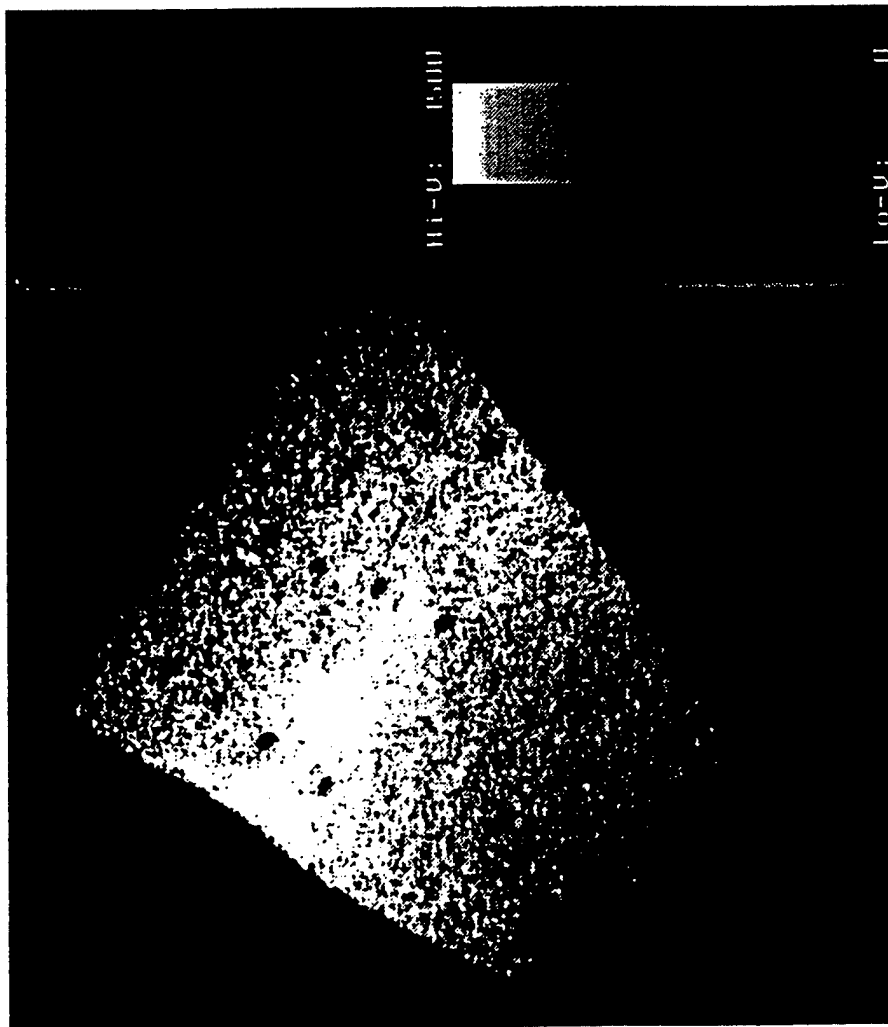


**Figure A.4** Qualitative PSP data reveals shock structure at 85% Nc, near-stall operating condition.



## APPENDIX B: Timing Calculation for Image Derotation

The gate time required to freeze the rotating image is calculated in this appendix. The desired spatial resolution is the parameter which defines the timing required to freeze the rotating image. For the timing calculation the desired spatial resolution was selected to be 1 mm.

N	Rotor mechanical speed, rpm
R	Rotor radius, m
$\Delta t$	Gate time, s
$\Delta X_b$	Blade movement during $\Delta t$ , m
$\Delta X_p$	Image pixel size, m

For a clear image, the blade must move less than  $\Delta X_p$  during  $\Delta t$ :

$$\Delta X_b = N \left( \frac{1 \text{ min}}{60 \text{ s}} \right) \frac{2\pi}{\text{revolution}} R \Delta t < \Delta X_p$$
$$N = 13,288 \text{ rpm (100\% } N_c)$$
$$R = 0.337 \text{ m}$$
$$\Delta X_p = 0.001 \text{ m}$$
$$\Delta t = 2.1 \mu\text{s}$$

Examination of the PSP test results revealed that the actual spatial resolution achieved was 0.1575 mm, for a total of 61,500 image points on the blade surface.

## APPENDIX C: Paint-Calibration Data

Figure C.1 shows the calibration curve of the original PSP developed at Wright Laboratory (WL) compared to the calibration curve of a typical porphyrin paint (PtOEP) obtained from Arnold Engineering and Development Center (AEDC). The WL paint displayed a 29% decrease in temperature sensitivity compared to typical phosphorescence-based paints. While the WL paint experiences a complete loss of pressure sensitivity after 80°C, the porphyrin displays a dramatic sensitivity to temperature; neither factor is compatible with turbomachinery applications. The following tables contain the calibration data of the PSP and TSP developed for the turbomachinery application presented in this thesis.

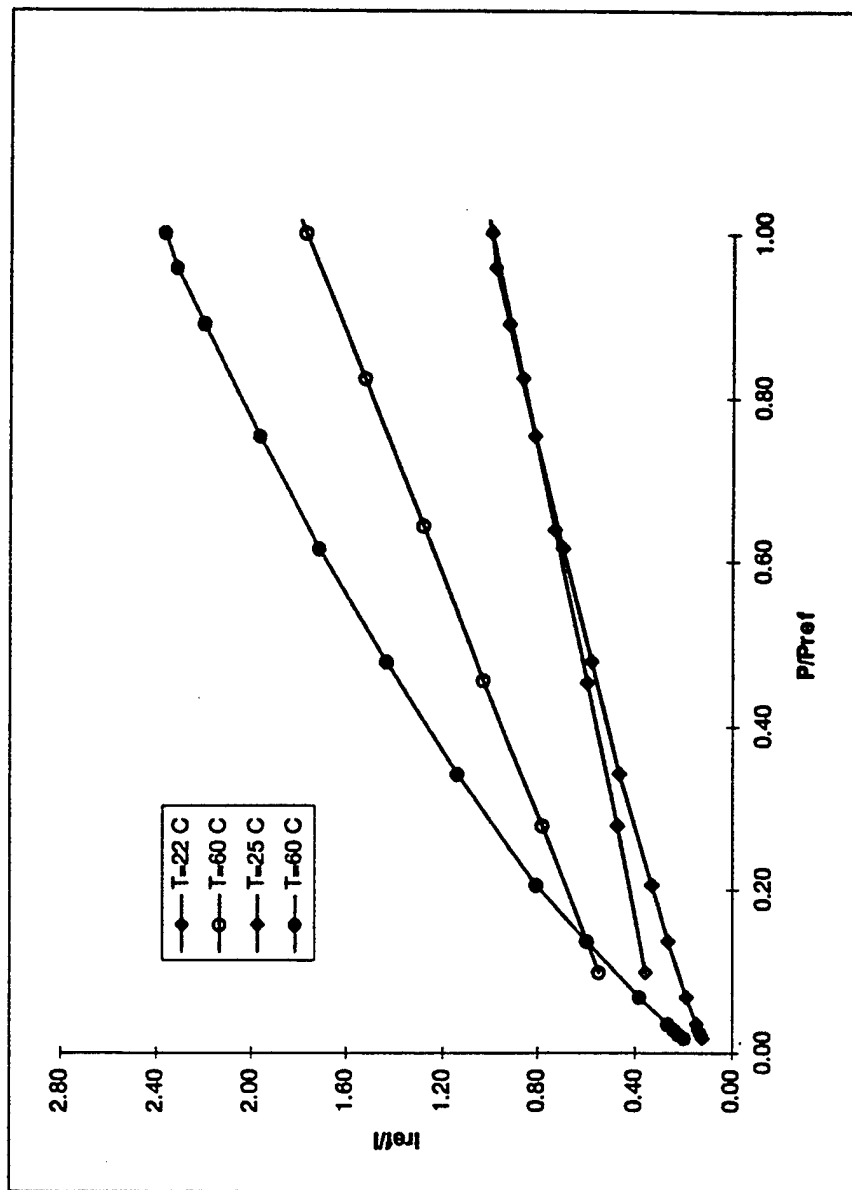


**Figure C.1** Performance of original WL PSP(open symbols) compared to a typical porphyrin paint (solid symbols).

# Temperature-Sensitive-Paint Calibration Data:

<u>T (C)</u>	<u>Intensity</u>	<u>Iref/I</u>	<u>ST (1/C)</u>	<u>ET (%T)</u>		
-12	78.132	0.863697	0.01866	4.4655		
-8	76.816	0.878502	0.01405	8.89855		
-3	74.579	0.904853	0.01014	32.8697		
2	72.053	0.936574	0.00756	66.12488	IREF=	67.483
7	69.829	0.966404	0.00587	24.34873	Tref=	17 C
12	69.333	0.973317	0.00481	17.34058		
17	67.483	1	0.00422	13.93431		
22	65.525	1.029882	0.00401	11.33832	d1=	0.93867
27	63.173	1.068225	0.00409	9.062233	d2=	0.007461 (1/C)
32	61.107	1.104342	0.00439	7.126448	d3=	-0.00016 (1/C)^2
37	58.995	1.143877	0.00484	5.588408	d4=	2.97E-06 (1/C)^3
42	56.473	1.19496	0.00537	4.429687	d5=	-9.00E-09 (1/C)^4
47	54.213	1.244775	0.00594	3.582844	R^2=	0.99919
52	52.194	1.292926	0.00647	2.972273		
57	50.171	1.34506	0.00692	2.534071		
62	47.943	1.407567	0.00726	2.220253		
67	45.781	1.474039	0.00748	1.996648		
72	43.622	1.546995	0.00755	1.839445		
77	41.624	1.621252	0.0075	1.73215		
82	39.465	1.709946	0.00733	1.663323		
87	37.192	1.814449	0.00707	1.624987		
92	35.035	1.92616	0.00674	1.611562		
97	32.869	2.05309	0.00637	1.619139		
102	30.834	2.188591	0.00596	1.645001		
107	28.834	2.340397	0.00554	1.687302		
112	26.69	2.5284	0.00512	1.744858		
117	24.886	2.711685	0.0047	1.817011		
122	22.754	2.965764	0.00431	1.903555		
127	21.29	3.169704	0.00393	2.004703		
132	20.07	3.362382	0.00357	2.121101		
137	18.947	3.561672	0.00324	2.253877		
142	18.117	3.724844	0.00293	2.404751		
147	17.411	3.875883	0.00264	2.57621		
152	16.853	4.004213	0.00237	2.771794		

Pressure-Sensitive-Paint Calibration Data:

Tref=-10.91 C Pref=99.16 Kpa Iref= 40.04

I	kPa	Temperatures C											
		-12	-6	0	5	12	15	20	25	30	35	40	
110.39	10.01	Iref/I 0.36	0.38	0.39	0.4	0.4	0.42	0.43	0.44	0.46	0.47	0.49	
94.87	19.04	0.42	0.45	0.46	0.48	0.48	0.51	0.52	0.54	0.56	0.57	0.61	
82.99	28.93	0.48	0.51	0.55	0.56	0.56	0.59	0.61	0.64	0.66	0.69	0.72	
74.8	39.07	0.54	0.57	0.61	0.63	0.63	0.67	0.69	0.72	0.75	0.78	0.82	
68.11	48.77	0.59	0.63	0.68	0.7	0.7	0.74	0.76	0.79	0.82	0.86	0.9	
63.39	58.99	0.63	0.68	0.73	0.75	0.75	0.8	0.82	0.86	0.89	0.94	0.98	
59.33	69	0.67	0.72	0.78	0.81	0.81	0.86	0.88	0.92	0.95	1	1.05	
56.21	78.98	0.71	0.77	0.83	0.85	0.86	0.91	0.94	0.98	1.01	1.05	1.1	
53.16	88.93	0.75	0.81	0.87	0.9	0.9	0.95	0.99	1.02	1.07	1.11	1.16	
50.9	98.96	0.79	0.85	0.91	0.94	0.94	1	1.03	1.07	1.12	1.16	1.22	
48.87	108.96	0.82	0.88	0.95	0.98	0.98	1.04	1.07	1.11	1.16	1.21	1.27	
47.06	118.96	0.85	0.92	0.99	1.02	1.02	1.08	1.12	1.15	1.21	1.25	1.32	
45.2	128.92	0.89	0.95	1.02	1.05	1.05	1.13	1.15	1.2	1.25	1.3	1.36	
43.92	138.95	0.91	0.98	1.05	1.08	1.09	1.16	1.2	1.23	1.28	1.35	1.4	
42.68	148.96	0.94	1.01	1.09	1.12	1.12	1.2	1.23	1.26	1.32	1.38	1.45	
41.43	158.96	0.97	1.04	1.11	1.15	1.15	1.24	1.27	1.3	1.35	1.42	1.48	
40.26	168.93	0.99	1.07	1.15	1.18	1.18	1.26	1.3	1.33	1.39	1.45	1.52	
39.3	178.97	1.02	1.09	1.17	1.21	1.21	1.3	1.33	1.36	1.42	1.49	1.56	
38.25	188.97	1.05	1.12	1.21	1.24	1.24	1.33	1.36	1.39	1.46	1.52	1.59	
37.37	198.91	1.07	1.15	1.23	1.27	1.26	1.36	1.39	1.41	1.49	1.55	1.63	

I	kPa	45	50	55	60	65	70	75	80	85	90	95	
110.39	10.01	0.51	0.53	0.55	0.57	0.6	0.63	0.66	0.68	0.71	0.74	0.77	
94.87	19.04	0.63	0.66	0.69	0.72	0.75	0.78	0.82	0.86	0.88	0.93	0.96	
82.99	28.93	0.75	0.78	0.82	0.85	0.89	0.93	0.98	1.02	1.07	1.1	1.15	
74.8	39.07	0.85	0.89	0.93	0.97	1.01	1.05	1.11	1.16	1.23	1.27	1.33	
68.11	48.77	0.94	0.98	1.02	1.07	1.12	1.17	1.23	1.28	1.36	1.43	1.48	
63.39	58.99	1.02	1.07	1.11	1.16	1.22	1.28	1.35	1.41	1.49	1.56	1.63	
59.33	69	1.09	1.14	1.19	1.25	1.31	1.37	1.44	1.51	1.59	1.67	1.76	
56.21	78.98	1.16	1.21	1.27	1.33	1.39	1.47	1.53	1.62	1.7	1.79	1.88	
53.16	88.93	1.22	1.27	1.34	1.4	1.47	1.55	1.63	1.72	1.81	1.91	2.01	
50.9	98.96	1.27	1.34	1.4	1.47	1.54	1.62	1.71	1.81	1.92	2.02	2.12	
48.87	108.96	1.33	1.39	1.46	1.54	1.61	1.7	1.8	1.89	2.02	2.12	2.24	
47.06	118.96	1.37	1.44	1.52	1.6	1.68	1.77	1.87	1.98	2.1	2.22	2.35	
45.2	128.92	1.42	1.5	1.57	1.66	1.74	1.83	1.95	2.07	2.18	2.31	2.45	
43.92	138.95	1.47	1.55	1.63	1.72	1.8	1.9	2.03	2.14	2.27	2.4	2.55	

42.68	148.96	1.51	1.6	1.68	1.78	1.87	1.97	2.09	2.21	2.35	2.5	2.65
41.43	158.96	1.56	1.64	1.73	1.82	1.92	2.04	2.16	2.28	2.43	2.59	2.76
40.26	168.93	1.6	1.68	1.78	1.86	1.98	2.09	2.22	2.35	2.52	2.67	2.84
39.3	178.97	1.64	1.73	1.82	1.91	2.03	2.15	2.27	2.42	2.59	2.74	2.93
38.25	188.97	1.67	1.76	1.86	1.96	2.08	2.21	2.33	2.47	2.65	2.84	3.01
37.37	198.91	1.71	1.81	1.9	2.02	2.14	2.26	2.41	2.55	2.73	2.92	3.1

I	kPa	100	105	110	115	120	125	130	135	140	145	150
110.39	10.01	0.79	0.83	0.86	0.87	0.9	0.94	0.98	1	1.04	1.08	1.12
94.87	19.04	1.01	1.07	1.1	1.14	1.15	1.19	1.3	1.33	1.35	1.43	1.46
82.99	28.93	1.23	1.3	1.34	1.39	1.45	1.51	1.59	1.66	1.72	1.8	1.87
74.8	39.07	1.42	1.5	1.56	1.62	1.71	1.78	1.86	1.94	2.04	2.11	2.22
68.11	48.77	1.6	1.69	1.75	1.83	1.94	2.02	2.11	2.21	2.31	2.42	2.54
63.39	58.99	1.76	1.87	1.94	2.04	2.14	2.24	2.34	2.47	2.58	2.7	2.84
59.33	69	1.91	2.03	2.12	2.22	2.34	2.47	2.58	2.7	2.82	2.99	3.13
56.21	78.98	2.06	2.17	2.28	2.41	2.51	2.67	2.81	2.95	3.07	3.24	3.4
53.16	88.93	2.22	2.32	2.44	2.58	2.7	2.87	3.02	3.16	3.32	3.49	3.65
50.9	98.96	2.37	2.47	2.6	2.74	2.89	3.05	3.22	3.38	3.57	3.75	3.92
48.87	108.96	2.49	2.62	2.77	2.93	3.07	3.24	3.41	3.61	3.78	3.98	4.18
47.06	118.96	2.61	2.74	2.91	3.08	3.25	3.4	3.59	3.78	4.02	4.23	4.39
45.2	128.92	2.73	2.88	3.04	3.22	3.39	3.58	3.76	4.02	4.21	4.43	4.67
43.92	138.95	2.84	3.03	3.17	3.38	3.59	3.77	3.95	4.19	4.44	4.67	4.88
42.68	148.96	2.98	3.15	3.31	3.53	3.75	3.93	4.15	4.39	4.61	4.9	5.12
41.43	158.96	3.09	3.25	3.45	3.66	3.88	4.1	4.32	4.56	4.81	5.12	5.3
40.26	168.93	3.2	3.4	3.59	3.8	4.06	4.29	4.48	4.78	4.98	5.3	5.54
39.3	178.97	3.31	3.5	3.73	4	4.19	4.45	4.63	4.93	5.2	5.5	5.77
38.25	188.97	3.41	3.66	3.87	4.13	4.33	4.59	4.82	5.1	5.38	5.67	5.97
37.37	198.91	3.51	3.76	3.96	4.25	4.48	4.76	5	5.27	5.59	5.88	6.16

Curve Fit to Pressure:

T	A	B (1/kPa)	C (1/kPa)^2
-12	0.323781034	0.005649573	-9.82013E-06
-6	0.335404028	0.006318604	-1.16504E-05
0	0.348262457	0.007003434	-1.33503E-05
5	0.358757542	0.007286738	-1.4144E-05
12	0.358118446	0.007295914	-1.42281E-05
15	0.369091729	0.007888037	-1.50951E-05
20	0.380768925	0.008184725	-1.60957E-05
25	0.392883742	0.008680593	-1.83533E-05
30	0.406659555	0.008999897	-1.85262E-05
35	0.420749238	0.009454289	-1.95127E-05

40	0.439114511	0.009963907	-2.07551E-05
45	0.452543554	0.010401778	-2.11818E-05
50	0.473482674	0.010862172	-2.16053E-05
55	0.49146949	0.011453584	-2.25815E-05
60	0.506090322	0.012171049	-2.394E-05
65	0.529559138	0.01260501	-2.36219E-05
70	0.552227184	0.013266247	-2.43086E-05
75	0.574927196	0.014057864	-2.53801E-05
80	0.590600427	0.015023165	-2.6966E-05
85	0.610892073	0.015872281	-2.70305E-05
90	0.636343445	0.016598362	-2.65595E-05
95	0.647159037	0.017740072	-2.79594E-05
100	0.647582528	0.020240834	-3.01465E-05
105	0.700454919	0.020670689	-2.75301E-05
110	0.70774122	0.022111465	-2.95526E-05
115	0.717305307	0.023478478	-2.95413E-05
120	0.720471269	0.02536804	-3.34072E-05
125	0.749266764	0.026627784	-3.36715E-05
130	0.782616323	0.028189203	-3.66514E-05
135	0.78554306	0.030270566	-3.97438E-05
140	0.794450238	0.032127412	-4.19566E-05
145	0.815828658	0.034161941	-4.47742E-05
150	0.843414176	0.035788774	-4.66267E-05

Curve Fit to Temperature:

<u>A(T)=</u>	<u>B(T)=</u>	<u>C(T)=</u>
a1=0.345870595	b1=0.00675378	c1=-1.30546E-05
a2=0.001546007	b2=7.93539E-05	c2=-1.93096E-07
a3=-5.04207E-06	b3=-2.41563E-07	c3=3.82606E-09
a4=1.01604E-06	b4=2.49928E-09	c4=-1.82414E-10
a5=-1.36305E-08	b5=8.42411E-11	c5=3.21931E-12
a6=6.7911E-11	b6=-4.03545E-13	c6=-2.29239E-14
a7=-1.15032E-13	b7=1.93804E-16	c7=5.57928E-17
R^2=0.99921178	R^2=0.999670177	R^2=0.997083386

PSP % Error in Pressure:

kPa	-12 C	12 C	40 C	70 C	100 C	130 C	150 C
10	2.64	2.63	3.02	3.64	3.65	4.10	4.11
30	1.55	1.65	1.98	2.43	2.73	3.26	3.55
50	1.45	1.61	1.99	2.46	2.91	3.60	4.07
70	1.51	1.72	2.17	2.69	3.28	4.11	4.75
90	1.62	1.90	2.43	3.00	3.71	4.70	5.51
100	1.70	2.01	2.59	3.18	3.95	5.02	5.91
120	1.87	2.27	2.98	3.61	4.47	5.69	6.76
140	2.09	2.61	3.50	4.13	5.06	6.41	7.67
160	2.38	3.07	4.24	4.80	5.72	7.20	8.66
180	2.75	3.74	5.43	5.70	6.50	8.08	9.75
200	3.27	4.85	7.72	7.04	7.44	9.07	10.98

PSP Sensitivity to Pressure (1/kPa):

kPa	-12 C	12 C	40 C	70 C	100 C	130 C	150 C
10	0.03790	0.03798	0.03315	0.02744	0.02737	0.02440	0.02434
30	0.02156	0.02024	0.01685	0.01370	0.01223	0.01021	0.00938
50	0.01379	0.01243	0.01006	0.00813	0.00686	0.00556	0.00492
70	0.00949	0.00831	0.00659	0.00532	0.00436	0.00347	0.00301
90	0.00685	0.00585	0.00457	0.00370	0.00299	0.00236	0.00202
100	0.00590	0.00498	0.00386	0.00314	0.00253	0.00199	0.00169
120	0.00445	0.00367	0.00279	0.00231	0.00186	0.00147	0.00123
140	0.00341	0.00273	0.00204	0.00173	0.00141	0.00111	0.00093
160	0.00263	0.00203	0.00147	0.00130	0.00109	0.00087	0.00072
180	0.00202	0.00148	0.00102	0.00097	0.00085	0.00069	0.00057
200	0.00153	0.00103	0.00065	0.00071	0.00067	0.00055	0.00046



## **APPENDIX D: Compressor Research Facility Background**

Figure D.1 is a layout of the Turbine Engine Research Center (TERC) Compressor Research Facility (CRF) located at Wright-Patterson Air Force Base. The facility consists of four buildings. Building 71B contains the control facilities and personnel offices, and Building 71D houses the water tower and cooling-water pumps. The test chamber, drive motors, and signal-conditioning room are housed in Building 20A, while the high-voltage equipment and frequency converters needed to power the drive motors are located in Building 20.

The CRF has an open-cycle design in which the test article provides the motive power to move air through the facility. The test article was mounted inside a 19.8-m-long, 6.1-m-diameter test chamber. Figure D.2 is a diagram of the test article installed in the CRF test chamber. Atmospheric air entered a plenum upstream of the test article after passing through the inlet filter house and an array of five throttling valves. These valves provided an inlet pressure to the test article that was proportionate to the drive system power. A flow-conditioning barrel mounted inside the plenum contained screens and flow straighteners to minimize distortion. From the plenum the air entered the test article bellmouth and passed through a set of inlet ducts before entering the fan. The facility can provide airflow rates in the range from 6.8 - 226.8 kg/sec to the test article.

Fan-core discharge flow passed through an instrumented diffuser and a core discharge valve (CDV) before being dumped into the facility exhaust collector. The CDV provided the discharge back pressure necessary for mapping compressor performance.

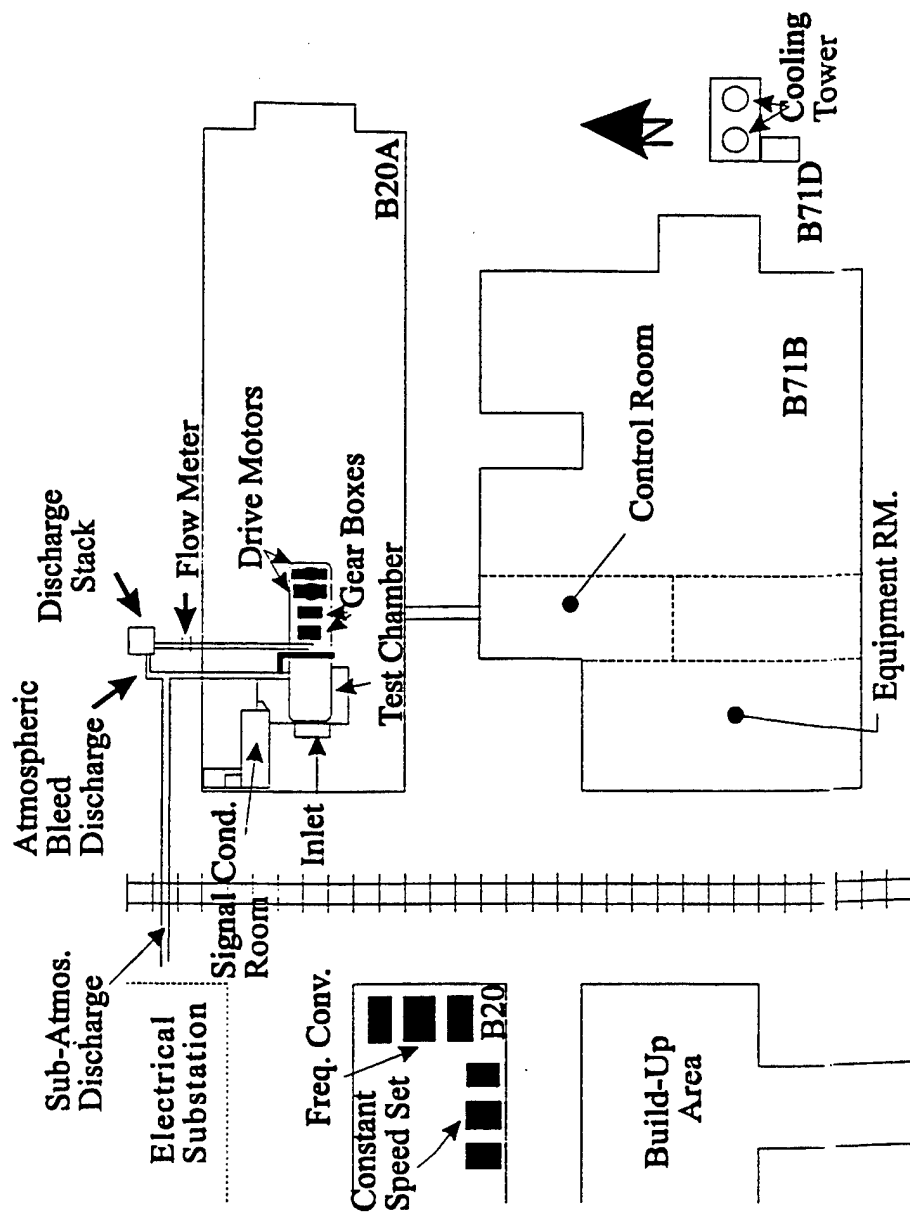


Figure D.1 Layout of the Compressor Research Facility.

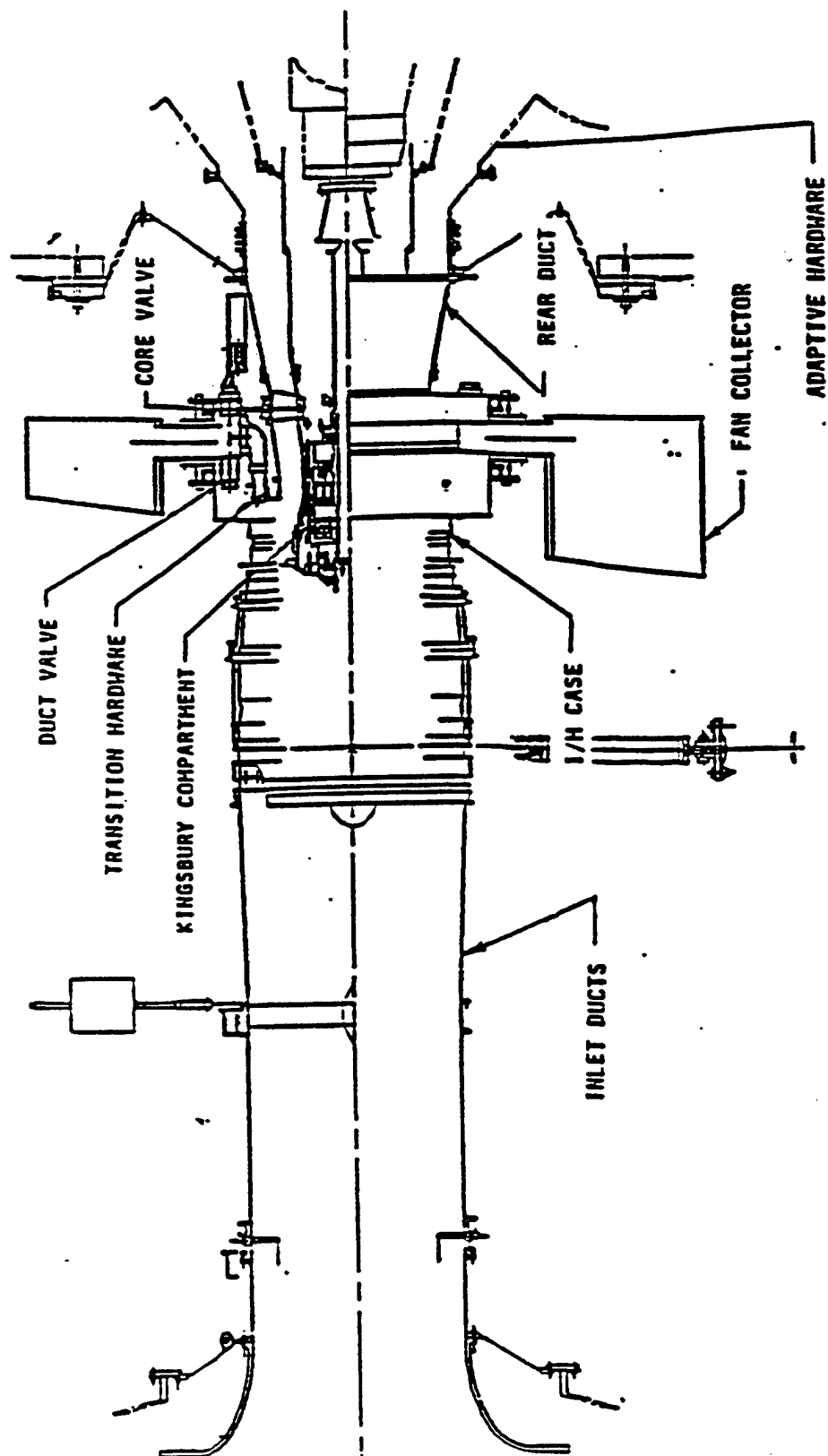


Figure D.2 Test chamber layout.

Fan by-pass discharge flow was routed through a by-pass flow collector and by-pass discharge valve (BDV) before entering the facility exhaust system. The BDV was used to provide the flow rate through the by-pass duct necessary to achieve a desired by-pass ratio. The discharge air flowed through separate venturis before being exhausted to the atmosphere through a noise-attenuating discharge stack. The compressor test was conducted with a 30-in.-diameter core flow venturi and a 0.48-m-diameter by-pass flow venturi.

The CRF powers its test articles through an electric drive system, which results in very accurately fixed rotational speeds. Municipal 60-Hz alternating-current electricity is converted to direct current before entering a frequency converter driven by a 9.25-MW motor-generator set. The test-article speed was controlled by varying the frequency of the power provided to the 22.37-MW synchronous electric motor. The test minimum rotational speed (min speed), the speed at which computers gain control of the rig, was 3,544 rpm.